The total virtual photoabsorption cross section, deeply virtual Compton scattering and vector-meson production[*]

M. Kuroda[1,2], D. Schildknecht[2]

[1] Institute of Physics, Meiji Gakuin University, Yokohama 244, Japan
[2] Fakultät für Physik, Universität Bielefeld, 33501 Bielefeld, Germany

Abstract. Based on the generic two-gluon-exchange dynamical mechanism for deeply inelastic scattering at low $x \simeq Q^2/W^2 \ll 1$, we stress the intimate direct connection between the total virtual photoabsorption cross section, deeply virtual Compton scattering and vector-meson electroproduction. A simple expression for the cross section for deeply virtual Compton scattering is derived. Parameter-free predictions are obtained for deeply virtual Compton forward scattering and vector-meson forward production, once the parameters in the total virtual photoabsorption cross section are determined in a fit to the experimental data on deeply inelastic scattering. Our predictions are compared with the experimental data from HERA.

1 Introduction

We have recently stressed and worked out [1,2] the intimate connection between deeply inelastic scattering (DIS) at $x \simeq Q^2/W^2 \ll 1$, i.e. between the virtual photoabsorption cross section including $Q^2 = 0$ photoproduction, and "elastic" diffractive production,

$$\gamma^* p \to (q\bar{q})^{J=1} p. \qquad (1.1)$$

In (1.1), $(q\bar{q})^{J=1}$ may refer to one of the discrete vector mesons, $\rho^0, \omega, \phi, J/\psi, \Upsilon$, or else, to the diffractively produced mass continuum under the restriction to spin $J = 1$. Deeply virtual Compton scattering, $\gamma^* p \to \gamma p$, is to be included in (1.1) by attaching a real photon to the final $(q\bar{q})^{J=1}$ state, via

$$\gamma^* p \to \left[\int (q\bar{q})^{J=1} \to \gamma \right] p, \qquad (1.2)$$

where the integration runs over the mass of the intermediate $(q\bar{q})^{J=1}$ state.

The treatment in [1,2] was relying on a single assumption: it is the generic two-gluon-exchange structure [3, 4] depicted in Figs. 1 and 2, that is the basic dynamical mechanism underlying the total photoabsorption cross section and diffractive production at low x.

In the present work we will employ the connection between the total photoabsorption cross section and diffractive production to obtain parameter-free predictions for deeply virtual Compton scattering, $\gamma^* p \to \gamma p$ (DVCS),
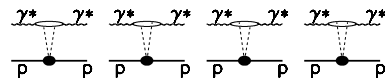

Fig. 1. The forward Compton amplitude

including real Compton scattering, $\gamma p \to \gamma p$, and for forward vector-meson electroproduction, including vector-meson photoproduction. Both, DVCS and vector-meson production, will be compared with the experimental data from HERA.

Section 2 summarizes the salient features of our approach to the total virtual photoabsorption cross section and diffractive production.

In Sect. 3, on the basis of Sect. 2, we will give a simple derivation of an extraordinarily simple expression for DVCS that will be shown to agree with the data [5] from HERA with respect to the W and the Q^2 dependence.

In Sect. 4, we turn to vector-meson production and compare with the experimental data [6] with respect to the W and the Q^2 dependence and the longitudinal-to-transverse ratio.
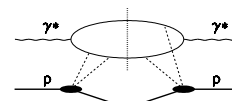
We end with brief conclusions in Sect. 5.

Fig. 2. One of the 16 diagrams for diffractive production. The vertical line indicates the unitarity cut corresponding to the diffractively produced final states, $(q\bar{q})^J$. Production of (discrete or continuum) vector states corresponds to $(q\bar{q})^J$ production with $J = 1$

2 The total virtual photoabsorption cross section

The intimate connection between the total photoabsorption cross section and "elastic" diffraction is explicitly represented by the recently derived sum rules [1,2]

$$\sigma_{\gamma_{\mathrm{T}}^* p}(W^2, Q^2) = \sqrt{16\pi} \sqrt{\frac{\alpha R_{e^+e^-}}{3\pi}}$$
$$\cdot \int_{m_0^2} \mathrm{d}M^2 \frac{M}{Q^2 + M^2} \sqrt{\left.\frac{\mathrm{d}\sigma_{\gamma_{\mathrm{T}}^* p \to (q\bar{q})_{\mathrm{T}}^{J=1} p}}{\mathrm{d}t \mathrm{d}M^2}\right|_{t=0}} \quad (2.1)$$

and

$$\sigma_{\gamma_{\mathrm{L}}^* p}(W^2, Q^2) = \sqrt{16\pi} \sqrt{\frac{\alpha R_{e^+e^-}}{3\pi}}$$
$$\cdot \int_{m_0^2} \mathrm{d}M^2 \frac{\sqrt{Q^2}}{Q^2 + M^2} \sqrt{\left.\frac{\mathrm{d}\sigma_{\gamma_{\mathrm{L}}^* p \to (q\bar{q})_{\mathrm{L}}^{J=1} p}}{\mathrm{d}t \mathrm{d}M^2}\right|_{t=0}}. \quad (2.2)$$

that relate the transverse and the longitudinal part of the total cross section to the transverse and the longitudinal part, respectively, of the forward-production amplitude of $(q\bar{q})^{J=1}$ (vector) states. The representations (2.1) and (2.2) follow from the assumption that the two-gluon-exchange dynamical mechanism of Figs. 1 and 2 be valid in the $x \to 0$ limit. The imaginary part of the $(q\bar{q})^{J=1}$-forward-production amplitude in (2.1) and (2.2) appears as the square root of the forward-production cross section[1,2]. We have

$$\left.\frac{\mathrm{d}\sigma_{\gamma_{\mathrm{T},\mathrm{L}}^* p \to (q\bar{q})_{\mathrm{T},\mathrm{L}}^{J=1} p}}{\mathrm{d}t \mathrm{d}M^2}\right|_{t=0}$$
$$= \left.\frac{\mathrm{d}\sigma_{\gamma_{\mathrm{T},\mathrm{L}}^* p \to (q\bar{q})_{\mathrm{T},\mathrm{L}}^{J=1} p}}{\mathrm{d}t \mathrm{d}M^2}\right|_{t=0} (W^2, Q^2, M^2). \quad (2.3)$$

As indicated in (2.3), the forward-production cross section depends on the total $\gamma^* p$ center-of-mass energy, W, and the photon four-momentum squared, $q^2 = -Q^2$, as well as the mass $M \equiv M_{q\bar{q}}$ of the $(q\bar{q})$ vector state being produced and integrated over in (2.1) and (2.2). The lower limit, m_0^2, in (2.1) and (2.2), with m_0 being smaller than the ρ^0-meson mass, $m_0^2 < m_{\rho^0}^2$, enters via quark–hadron duality [7–9]; the vector mesons, $\rho^0, \omega, \phi, J/\psi$ and Υ are treated as part of the diffractive continuum rather

---

[1]   Strictly speaking, forward production of (massive) $(q\bar{q})$ vector states involves a finite momentum transfer, $|t_{\min}|$, and the sum rules (2.1) and (2.2) require an extrapolation to $t = 0$. We will employ the approximation of $|t_{\min}| \simeq 0$ for diffractive forward production, since $|t_{\min}|$ becomes exceedingly small for $x \to 0$. Compare the explicit formula for $|t_{\min}|$ in Sect. 4

[2]   In (2.1) and (2.2), we have suppressed factors $1/\sqrt{(1+\beta_{\mathrm{T}}^2)}$ and $1/\sqrt{(1+\beta_{\mathrm{L}}^2)}$, respectively, where $\beta_{\mathrm{T},\mathrm{L}}$ stands for the ratio of the real-to-imaginary part of the forward-scattering amplitude. The ratio $\beta_{\mathrm{T},\mathrm{L}}$ is expected to be small, $\beta_{\mathrm{T},\mathrm{L}} \ll 1$, as in truly elastic hadron–hadron scattering, and $\beta_{\mathrm{T},\mathrm{L}}^2$ may frequently be ignored.

than being added as separate resonances. Indeed, photoabsorption for spacelike photons should be insensitive to fine details of the photon coupling to $q\bar{q}$ pairs in the timelike region and a global description in which a continuous spectral weight function interpolates [8] the low-lying vector-meson resonances is expected to be successful. The sum of the squares of the active quark charges (in units of e) in (2.1) and (2.2) is expressed by

$$R_{e^+e^-} = 3 \sum_q Q_q^2, \quad (2.4)$$

where $R_{e^+e^-}$ denotes the cross section for e^+e^- annihilation, $R_{e^+e^-} \to (q\bar{q})^{J=1} \to$ hadrons, in units of the cross section for $e^+e^- \to \mu^+\mu^-$.

The sum rules (2.1) and (2.2) were derived [1,2] by comparing with each other the explicit expressions for the total cross section and the cross section for diffractive production based on the two-gluon-exchange interaction depicted in Figs. 1 and 2 in the limit of $x \simeq Q^2/W^2 \ll 1$. In the frequently employed transverse-position-space representation [10,4] the total cross section and the cross section for diffractive production of $(q\bar{q})^{J=1}$ (vector) states are then given by [2,1]

$$\sigma_{\gamma_{\mathrm{T},\mathrm{L}}^* p}(W^2, Q^2)$$
$$= \int \mathrm{d}z \int \mathrm{d}^2 r_\perp |\psi_{\mathrm{T},\mathrm{L}}(r_\perp, z(1-z), Q^2)|^2$$
$$\cdot \sigma_{(q\bar{q})_{\mathrm{T},\mathrm{L}}^{J=1} p}(r_\perp \sqrt{z(1-z)}, W^2) \quad (2.5)$$

and

$$\left.\frac{\mathrm{d}\sigma_{\gamma_{\mathrm{T},\mathrm{L}}^* p \to (q\bar{q})_{\mathrm{T},\mathrm{L}}^{J=1} p}}{\mathrm{d}t}\right|_{t=0}$$
$$= \frac{1}{16\pi} \int \mathrm{d}z \int \mathrm{d}^2 r_\perp \left|\psi_{\mathrm{T},\mathrm{L}}(r_\perp, z(1-z), Q^2)\right|^2$$
$$\cdot \sigma_{(q\bar{q})_{\mathrm{T},\mathrm{L}}^{J=1} p}^2(r_\perp \sqrt{z(1-z)}, W^2), \quad (2.6)$$

where

$$\sigma_{(q\bar{q})_{\mathrm{T},\mathrm{L}}^{J=1}}(\mathbf{r}_\perp \sqrt{z(1-z)}, W^2)$$
$$= \int \mathrm{d}^2 l'_\perp \bar{\sigma}_{(q\bar{q})_{\mathrm{T},\mathrm{L}}^{J=1} p}(\mathbf{l}_\perp'^2, W^2)$$
$$\cdot (1 - e^{-i\mathbf{l}_\perp' \cdot \mathbf{r}_\perp \sqrt{z(1-z)}}). \quad (2.7)$$

In (2.5), the restriction that the photon exclusively couples to spin $J = 1$ quark–antiquark pairs, $(q\bar{q})^{J=1}$, is explicitly incorporated. The dependence of the color-dipole cross section, $\sigma_{(q\bar{q})_{\mathrm{T},\mathrm{L}}^{J=1}}(r_\perp \sqrt{z(1-z)}, W^2)$ on $r_\perp \sqrt{z(1-z)}$ assures the restriction to the scattering of $J = 1$ color dipoles on the proton. As usual, in (2.5) and (2.6) the (light-cone) wave function of the virtual photon is denoted by $\psi_{\mathrm{T},\mathrm{L}}(r_\perp, z(1-z), Q^2)$, where

$$\left|\psi_{\mathrm{T}}(r_\perp, z(1-z), Q^2)\right|^2$$
$$= \frac{6\alpha}{(2\pi)^2} \sum_q Q_q^2 \left[\left(z^2 + (1-z)^2\right) \epsilon^2 K_1(\epsilon r_\perp)^2\right]$$

$$+ m_q^2 K_0(\epsilon r_\perp)^2], \qquad (2.8)$$

$$\left|\psi_{\mathrm{L}}(r_\perp, z(1-z), Q^2)\right|^2$$
$$= \frac{6\alpha}{(2\pi)^2} \sum_q Q_q^2 \left[4Q^2 z^2(1-z)^2 K_0(\epsilon r_\perp)^2\right], \quad (2.9)$$

$$\epsilon^2 = z(1-z)Q^2 + m_q^2. \qquad (2.10)$$

In standard notation, Q_q and m_q denote the quark charge and mass, respectively, and z is the fraction of the light-cone momentum carried by the quark from the $q\bar{q}$ pair, i.e. $k_+ = zq_+ = z(q^0 + q^3)$. Finally, K_1 and K_0 denote modified Bessel functions.

Upon inserting (2.7) into (2.5) and (2.6) and introducing the mass of the $(q\bar{q})^{J=1}$ state, $M \equiv M_{(q\bar{q})^{J=1}}$, and upon reducing the number of integrations, one reads off the validity of the sum rules (2.1) and (2.2)[3].

The representations (2.5) to (2.7) differ from the frequently employed ones [4]

$$\sigma_{\gamma^*_{\mathrm{T,L}} p}(W^2, Q^2)$$
$$= \int \mathrm{d}z \int \mathrm{d}^2 r_\perp \left|\psi_{\mathrm{T,L}}(r_\perp, z(1-z), Q^2)\right|^2$$
$$\cdot \sigma_{(q\bar{q})p}(\mathbf{r}_\perp, W^2), \qquad (2.11)$$

and

$$\left.\frac{\mathrm{d}\sigma_{\gamma^*_{\mathrm{T,L}} p \to Xp}(W^2, Q^2)}{\mathrm{d}t}\right|_{t=0}$$
$$= \frac{1}{16\pi} \int \mathrm{d}z \int \mathrm{d}^2 r_\perp \left|\psi_{\mathrm{T,L}}(r_\perp, z(1-z), Q^2)\right|^2$$
$$\cdot \sigma_{(q\bar{q})p}^2(\mathbf{r}_\perp, W^2), \qquad (2.12)$$

with[4]

$$\sigma_{(q\bar{q})p}(r_\perp, W^2) = \int \mathrm{d}^2 l_\perp \tilde{\sigma}_{(q\bar{q})p}\left(\mathbf{l}_\perp^2, W^2\right)\left(1 - e^{-i\mathbf{l}_\perp \cdot \mathbf{r}_\perp}\right)$$
$$(2.13)$$

by the substitutions[5]

$$\mathbf{r}_\perp \to \mathbf{r}_\perp' = \mathbf{r}_\perp \sqrt{z(1-z)},$$
$$\mathbf{l}_\perp \to \mathbf{l}_\perp' = \frac{\mathbf{l}_\perp}{\sqrt{z(1-z)}}, \qquad (2.14)$$

and

$$z(1-z)\tilde{\sigma}_{(q\bar{q})p}(\mathbf{l}_\perp'^2 z(1-z), W^2) \to \bar{\sigma}_{(q\bar{q})^{J=1}_{\mathrm{T,L}} p}(\mathbf{l}_\perp'^2, W^2).$$
$$(2.15)$$

---

[3] The approximation of massless quarks was employed throughout.

[4] Note that $\ell_\perp^4 \tilde{\sigma}_{(q\bar{q})p}(\ell_\perp^2, W^2)$ in (2.13) is proportional to the gluon density theoretically examined in BFKL approach [11], and phenomenologically investigated in [12]. In the present investigation we are only concerned with the spin $J=1$ projection of $\tilde{\sigma}_{(q\bar{q})p}(\ell_\perp^2, W^2)$ and, consistent with the mass dispersion relation of GVD, we adopt W^2 as the basic variable rather than $x \sim Q^2/W^2$.

[5] The momentum $\ell_\perp' = \ell_\perp/\sqrt{z(1-z)}$ is the momentum of the gluon that is absorbed by the quark of momentum $\mathbf{k}_\perp/\sqrt{z(1-z)}$. when transversing the nucleon.

The replacement defined by (2.14) and (2.15) is a consequence of applying a partial-wave decomposition of the $q\bar{q}$ states in (2.11) to (2.13). The partial-wave decomposition explicitly eliminates all contributions of $(q\bar{q})^{J\neq 1}$ states that are irrelevant in (2.11), since they are projected to zero by the square of the photon wave function. The elimination of these redundant components of the dipole cross section is of particular importance, if the experimental data on $\sigma_{\gamma^* p}(W^2, Q^2)$ are used to extract the dipole cross section by employing a fitting procedure.

A fit based on (2.5) yields a unique prediction, according to (2.6), for the (whole) diffractive production of $(q\bar{q})^{J=1}_{\mathrm{T,L}}$ states. A fit based on (2.11), however, does *not* yield a prediction for diffractive production according to (2.12). The contributions from diffractively produced states $(q\bar{q})^{J\neq 1}$, necessarily included in (2.12), remain unconstrained in a fit based on (2.11). The fact that various different dipole cross sections [13] lead to equally good representations of $\sigma_{\gamma^* p}(W^2, Q^2)$ is presumably a consequence of the presence of such $J \neq 1$ contributions that remained undetermined in the fits to $\sigma_{\gamma^* p}(W^2, Q^2)$. The representation (2.11) by itself is highly non-unique with respect to the color-dipole cross section. The alternative of a simultaneous fit of (2.11) and (2.12) would have to cope with the much larger experimental uncertainty of the experimental data on diffractive production in comparison with the ones on $\sigma_{\gamma^* p}(W^2, Q^2)$. It is preferable, accordingly, with respect to fits of experimental data to use the representation (2.5) with (2.7), and turn to a description of the total diffractive production that includes $(q\bar{q})^{J\neq 1}$ states subsequently.

Coming back to the sum rules (2.1) and (2.2) for a moment, we note that they can be written down directly, without referring to the two-gluon-exchange dynamics, provided one is willing to adopt the validity of generalized vector dominance (GVD [14,8]), and (2.1) was indeed first given from GVD [15]. In terms of GVD, the factor

$$\sqrt{\frac{\alpha R_{e^+e^-}}{3\pi} \frac{1}{M^2}} \frac{M^2}{Q^2 + M^2} \qquad (2.16)$$

in (2.1) originates from the coupling of the photon to the $(q\bar{q})^{J=1}$ intermediate state in Fig. 2 and its propagation (always assuming $x \to 0$), once a virtual photon, γ^*_{T}, is attached to it, in order to reproduce the corresponding diagram of Fig. 1. In the case of the longitudinal photon, γ^*_{L}, in (2.2), an additional factor $\sqrt{Q^2/M^2}$ must be included in GVD [16,14] as a consequence of the coupling of the photon to a conserved source.

An additional general comment may be appropriate at this point concerning the emergence of GVD as a consequence of the two-gluon-exchange dynamical mechanism of Fig. 1 in the $x \to 0$ limit. The essential point is the observation, by no means new [17,4,18], that the denominators of the quark propagators in Fig. 1 in the $x \to 0$ limit in the photoabsorption cross section lead to factors of the form

$$\frac{1}{Q^2 + M^2}, \qquad (2.17)$$

with

$$M^2 = M^2_{q\bar{q}} = \frac{\mathbf{k}^2_\perp + m^2_q}{z(1-z)}. \qquad (2.18)$$

In (2.17), one recognizes the denominator of a vector-meson propagator for a vector-meson $(q\bar{q})$ state of mass M. Note that the propagator mass $M_{q\bar{q}}$ in (2.18) is related to the spacelike four-momentum squared q^2 of the photon the $q\bar{q}$ pair is coupled to,

$$q^2 = \frac{k^2_q + \mathbf{k}^2_\perp}{z} + \frac{k^2_{\bar{q}} + \mathbf{k}^2_\perp}{1-z} = -Q^2 < 0, \qquad (2.19)$$

by substitution of the on-shell values

$$k^2_q = k^2_{\bar{q}} = m^2_q, \qquad (2.20)$$

for both the quark and the antiquark four-momentum. The $q\bar{q}$ mass in the propagator, i.e. the mass of the $q\bar{q}$ state the photon dissociates or "fluctuates" into, is accordingly identical to the mass of a $q\bar{q}$ state (with on-shell quarks) diffractively produced via two-gluon exchange. In short, the quark propagator becomes transmogrified into a vector-meson propagator containing the invariant mass (2.18) of a system of an on-shell quark and an on-shell antiquark, i.e. we have the GDV structure.

So far, no specific realization of the lower vertex in Figs. 1 and 2 was adopted. Examining the dipole cross section (2.7) in the limit of large and small interquark separation, $r'_\perp \to \infty$ and $r'_\perp \to 0$, allows one to strongly reduce arbitrariness. From (2.7)[6],

$$\sigma_{(q\bar{q})^{J=1}p}(r'_\perp, W^2) = \sigma^{(\infty)}(W^2)$$
$$\cdot \begin{cases} 1, & \text{for } r'_\perp \to \infty, \\ \frac{1}{4}r'^2_\perp \langle \mathbf{l}'^2_\perp \rangle_{W^2}, & \text{for } r'^2_\perp \langle \mathbf{l}'^2_\perp \rangle_{W^2} \to 0, \end{cases} \qquad (2.21)$$

where

$$\sigma^{(\infty)}(W^2) = \pi \int d\mathbf{l}'^2_\perp \bar{\sigma}_{(q\bar{q})^{J=1}}(\mathbf{l}'^2_\perp, W^2), \qquad (2.22)$$

and

$$\langle \mathbf{l}'^2_\perp \rangle_{W^2} = \frac{\int d\mathbf{l}'^2_\perp \mathbf{l}'^2_\perp \bar{\sigma}_{(q\bar{q})^{J=1}}(\mathbf{l}'^2_\perp, W^2)}{\int d\mathbf{l}'^2_\perp \bar{\sigma}_{(q\bar{q})^{J=1}}(\mathbf{l}'^2_\perp, W^2)}$$
$$\equiv \Lambda^2(W^2), \qquad (2.23)$$

we find that the $J = 1$ color-dipole cross section is strongly constrained, once the integral (2.22) over the gluon-momentum dependence and its first moment, (2.23), the "saturation scale", $\Lambda^2(W^2)$, are specified. Even though given values of the energy-dependent quantities $\sigma^{(\infty)}(W^2)$ and $\langle \mathbf{l}'^2_\perp \rangle_{W^2} \equiv \Lambda^2(W^2)$ do by no means uniquely specify

the color-dipole cross section, different functional forms of $\sigma_{(q\bar{q})^{J=1}p}(r'_\perp, W^2)$ restricted by identical integrated distributions (2.22) and (2.23) are nevertheless largely equivalent. According to (2.21) they lead to identical color-dipole cross sections in both the limit of large and the limit of small interquark separation.

The ansatz for the $J = 1$ color-dipole cross section chosen previously (generalized vector dominance-color-dipole picture, GVD-CDP) [19] is parametrized in terms of $\sigma^{(\infty)}(W^2)$ and $\Lambda^2(W^2)$,

$$\bar{\sigma}_{(q\bar{q})^{J=1}_T}(\mathbf{l}'^2_\perp, W^2)$$
$$= \bar{\sigma}_{(q\bar{q})^{J=1}_L}(\mathbf{l}'^2_\perp, W^2)$$
$$= \sigma^{(\infty)}(W^2) \cdot \frac{1}{\pi}\delta(\mathbf{l}'^2_\perp - \Lambda^2(W^2)), \qquad (2.24)$$

and it can indeed be adopted without significant loss of generality. In other words, the ansatz (2.24) that parametrizes the $J = 1$ color-dipole cross section in terms of the two W-dependent parameters (2.22) and (2.23) is a fairly stringent consequence from the underlying two-gluon-exchange mechanism. The specific choice of the δ-function in (2.24) is a purely technical simplification.

With respect to transverse position space, according to (2.7) and (2.24) becomes

$$\sigma_{(q\bar{q})^{J=1}p}(\mathbf{r}'^2_\perp, W^2) = \sigma^{(\infty)}(W^2)(1 - J_0(r'_\perp \Lambda(W^2))), \qquad (2.25)$$

where $J_0(r'_\perp \Lambda(W^2))$ denotes a Bessel function.

A general conclusion on the energy dependence of the total cross section follows immediately upon substituting (2.21) into (2.7) and subsequently (2.7) into the expression for the total cross section (2.5). Provided we exclude the (artificial) assumption that the first moment of the transverse-momentum distribution (2.23) be independent of W, i.e. provided we exclude the assumption of $\Lambda^2(W^2) = \text{const.}$, the increasing importance in (2.5) of the short-distance limit (2.21) with increasing Q^2 will imply an increasingly stronger dependence of $\sigma_{\gamma^*p}(W^2, Q^2)$ on W. This is indeed, what is observed experimentally [20].

A theoretical argument against $\Lambda^2(W^2) = \text{constant}$ may also be based on requiring duality between the two-gluon-exchange dynamics and Regge (or more specifically pomeron) behavior in the $Q^2 = 0$ photoproduction limit. Requiring the energy dependence in photoproduction from (2.5) and (2.25) to coincide with the one due to pomeron exchange,

$$\sigma^{\text{pomeron}}_{\gamma p}(W^2)$$
$$\equiv \sigma^{(\infty)}(W^2) \int dz \int d^2r_\perp \left| \psi_T(r_\perp, z(1-z), Q^2 = 0) \right|^2$$
$$\cdot \left(1 - J_0\left(r_\perp\sqrt{z(1-z)}\Lambda(W^2)\right)\right), \qquad (2.26)$$

and to be a genuine consequence of the generic two-gluon-exchange structure[7], a factorized W dependence, unre-

---

[6] It is to be stressed that "saturation" for $r'_\perp \to \infty$ and "color transparency" for $r'_\perp \to 0$ in (2.21) are a consequence of the QCD-gauge-theory structure that is contained in (2.7). Compare [4]. Also, we drop the indices T,L, anticipating the ansatz (2.24) that does not contain a dependence on whether the $(q\bar{q})^{J=1}$ state is transversely or longitudinally polarized.

[7] The smooth transition to photoproduction may also be used as an argument for the dipole cross section in (2.21) to

lated to the structure of the two-gluon-exchange dynamics that is contained in the integral in (2.26), is theoretically disfavored. In other words, the option $\Lambda = $ constant that imposes soft-pomeron behavior by an overall factor in (2.26) may safely be dismissed on theoretical grounds.

The theoretical argument is supported by a fit [19] to the experimental data [20] that uses the parameterization of $\sigma_{\gamma p}(W^2)$ by pomeron exchange as an input at $Q^2 = 0$, thus replacing $\sigma^{(\infty)}(W^2)$ by $\sigma_{\gamma p}^{\text{pomeron}}$ according to (2.26). The fit to the experimental data indeed gave an increase of $\Lambda^2(W^2)$ with W^2, while $\sigma^{(\infty)}$ turned out to be energy independent in good approximation.

In momentum space, the ansatz (2.24), (2.25) for the total cross section (2.5) implies [1]

$$\sigma_{\gamma_T^* p}(W^2, Q^2) = \frac{\alpha R_{e^+e^-}}{3\pi} \sigma^{(\infty)} \int_{m_0^2} dM^2 \frac{1}{Q^2 + M^2}$$

$$\cdot \left[\frac{M^2}{Q^2 + M^2} \right.$$

$$\left. - \frac{1}{2} \left(1 + \frac{M^2 - \Lambda^2(W^2) - Q^2}{\sqrt{(Q^2 + M^2 - \Lambda^2(W^2))^2 + 4Q^2\Lambda^2(W^2)}} \right) \right]$$

(2.27)

and

$$\sigma_{\gamma_L^* p}(W^2, Q^2) = \frac{\alpha R_{e^+e^-}}{3\pi} \sigma^{(\infty)} \int_{m_0^2} dM^2 \frac{1}{Q^2 + M^2}$$

$$\cdot \left[\frac{Q^2}{Q^2 + M^2} \right.$$

$$\left. - \frac{Q^2}{\sqrt{(Q^2 + M^2 - \Lambda^2(W^2)) + 4Q^2\Lambda^2(W^2))}} \right].$$

(2.28)

The result of the integration of (2.27) and (2.28) was given before [1]. Here, in connection with the procedure used in Sects. 3 and 4, it is useful to note that the $Q^2 \to 0$ and the $Q^2 \gg \Lambda^2(W^2)$ limit of $\sigma_{\gamma_{T,L}^* p}(W^2, Q^2)$ can immediately be derived by taking the corresponding limits under the integrals in (2.27) and (2.28). For $Q^2 \ll \Lambda^2(W^2)$, or, equivalently, $\eta \ll 1$, one finds

$$\sigma_{\gamma^* p}(W^2, Q^2) = \frac{\alpha}{3\pi} R_{e^+e^-} \sigma^{(\infty)} \ln \frac{1}{\eta}, \qquad (2.29)$$

while for $Q^2 \gg \Lambda^2(W^2)$, or $\eta \gg 1$,

$$\sigma_{\gamma_T^* p}(W^2, Q^2) = 2\sigma_{\gamma_L^* p}(W^2, Q^2)$$

$$= \frac{\alpha}{3\pi} R_{e^+e^-} \sigma^{(\infty)} \frac{1}{3\eta}, \qquad (2.30)$$

with the scaling variable [21]

$$\eta(W^2, Q^2) = \frac{Q^2 + m_0^2}{\Lambda^2(W^2)}. \qquad (2.31)$$

The fit to the experimental data with the ansatz (2.24) gave [22][8]

$$\Lambda^2(W^2) = \begin{cases} B \left(\frac{W^2}{W_0^2} + 1 \right)^{C_2}, \\ C_1' \ln \left(\frac{W^2}{W_0'^2} + C_2' \right), \end{cases}$$

$$m_0^2 = 0.15 \pm 0.04 \, \text{GeV}^2, \qquad (2.32)$$

where

$$B = 2.24 \pm 0.43 \, \text{GeV}^2,$$
$$W_0^2 = 1081 \pm 124 \, \text{GeV}^2,$$
$$C_2 = 0.27 \pm 0.01. \qquad (2.33)$$

We emphasize the emergence of a "soft" energy dependence in (2.29) and a "hard" one in (2.30) as a strict consequence of the generic two-gluon-exchange dynamics together with the natural assumption that the effective gluon transverse momentum (2.23) is to increase with energy W.

Note that the normalization of the cross sections (2.27) to (2.30) is determined by the product $R_{e^+e^-} \sigma^{(\infty)}$. With $R_{e^+e^-} = 2$ for three active flavors, relevant for photoproduction, the experimental data require [19]

$$\sigma^{(\infty)} = 30 \, \text{mb} \simeq 77.04 \, \text{GeV}^{-2}. \qquad (2.34)$$

With respect to the treatment of vector-meson production in Sect. 3, we also note the cross section for diffractive production. With the ansatz (2.21) and (2.6), one obtains [1]

$$\frac{d\sigma_{\gamma_T^* p \to (q\bar{q})_T^{J=1}}}{dt\, dM^2 dz} \bigg|_{t=0}$$

$$= \frac{\alpha \cdot R_{e^+e^-}}{3 \cdot 16\pi^2} (\sigma^{(\infty)})^2 \frac{3}{2} \left(z^2 + (1-z)^2 \right) \frac{1}{M^2}$$

$$\cdot \left[\frac{M^2}{Q^2 + M^2} - \frac{1}{2} \left(1 \right.\right.$$

$$\left.\left. + \frac{M^2 - \Lambda^2(W^2) - Q^2}{\sqrt{(Q^2 + M^2 - \Lambda^2(W^2))^2 + 4Q^2\Lambda^2(W^2)}} \right) \right]^2,$$

(2.35)

and

$$\frac{d\sigma_{\gamma_L^* p \to (q\bar{q})_L^{J=1}}}{dt\, dM^2 dz} \bigg|_{t=0}$$

$$= \frac{\alpha \cdot R_{e^+e^-}}{3 \cdot 16\pi^2} (\sigma^{(\infty)})^2 \cdot 6Q^2 z(1-z)$$

---

[8] We note that the energy scale W_0 may be eliminated in favor of $Q^2 \equiv Q_0^2 = 1 \, \text{GeV}^2$ and the value of x corresponding to W_0^2 and Q_0^2, i.e. $x_0 \equiv Q_0^2/W_0^2$. We have in very good approximation

$$\Lambda^2(W^2) \cong B x_0^{C_2} \left(\frac{W^2}{1 \, \text{GeV}^2} \right)^{C_2} = 0.340 \left(\frac{W^2}{1 \, \text{GeV}^2} \right)^{0.27} \text{GeV}^2.$$

(2.23) to depend on the single variable $W^2 = x/Q^2$ rather than on x, or on both x and Q^2 independently. Note that in addition to the propagator factor (2.17), it is the dependence of the dipole cross section on the single variable W that fully guarantees the GVD structure.

$$\cdot \left[\frac{1}{Q^2 + M^2} \right.$$

$$\left. - \frac{1}{\sqrt{(Q^2 + M^2 - \Lambda^2(W^2))^2 + 4Q^2\Lambda^2(W^2)}} \right]^2 ,$$

(2.36)

and, finally, for the sum of (2.35) and (2.36),

$$\frac{d\sigma_{\gamma^*p \to (q\bar{q})^{J=1}p}}{dt dM^2} \bigg|_{t=0} = \frac{\alpha R_{e^+e^-}}{3 \cdot 32\pi^2} (\sigma^{(\infty)})^2 \frac{1}{M^2}$$

$$\cdot \left[1 - \frac{(M^2 + Q^2)^2 - (M^2 - Q^2)\Lambda^2(W^2)}{(M^2 + Q^2)\sqrt{(Q^2 + M^2 - \Lambda^2(W^2))^2 + 4Q^2\Lambda^2(W^2)}} \right].$$

(2.37)

Comparing (2.35) and (2.36) with (2.27) and (2.28) once again takes us back to the sum rules (2.1) and (2.2), now based on the specification (2.21) of the $J = 1$ color-dipole cross section.

From (2.29), for any fixed Q^2, for $W \to \infty$, we have "saturation" in the sense of reaching the photoproduction limit [21, 22],

$$\lim_{\substack{W^2 \to \infty \\ Q^2 = \text{const}}} \frac{\sigma_{\gamma^*p}(W^2, Q^2)}{\sigma_{\gamma p}(W^2)} = 1.$$

(2.38)

We add a brief comment on the relation of our approach to the one in [12,23]. In [12,23], the $\ell_\perp$-factorization representation (2.11) and (2.12) is implemented by relating the unintegrated gluon distribution at sufficiently large Q^2 to the empirically determined integrated gluon distribution, and by applying a suitable extrapolation to reach the limit of Q^2 towards zero. Our approach starts by carrying out the $J = 1$ projection implicitly contained in (2.11) and (2.12), and it specifies the $J = 1$ part of the color-dipole cross section, compare (2.21) to (2.25), in a manner consistent with the scaling law [21, 22], $\sigma_{\gamma^*p} = \sigma_{\gamma^*p}(\eta)$. The underlying gluon distribution in our approach may be constructed by taking the logarithmic derivative of the structure function, $F_2 \approx Q^2 \sigma_{\gamma^*p}$, following [24].

It has been the aim of this Sect. 2 to prepare the ground for the discussions on DVCS and on "elastic" diffraction, in particular vector-meson production, in Sects. 3 and 4. The exposition of Sect. 2 was meant to show that hardly any additional assumption need to be introduced to reach a quantitative[9] description of the experimental data on $\sigma_{\gamma^*p}(W^2, Q^2)$, once the $x \to 0$ limit of the generic two-gluon-exchange mechanism is adopted.

3 Deeply virtual Compton scattering

With the results from Sect. 2, it is a simple matter to deduce the forward-scattering amplitude and the forward-

scattering cross section for DVCS. The reaction $\gamma^*p \to \gamma p$ is described by the diagrams in Fig. 1 upon putting the final photon, γ, on-shell, $Q^2 = 0$.

Technically, three different, but equivalent, ways suggest themselves to derive the (dominant) imaginary part of the DVCS amplitude.

(i) Evaluate the representation (2.5) for the transverse part[10] of the total virtual photoabsorption cross section upon substituting $Q^2 = 0$ in one of the photon wave functions, $\psi_T(r_\perp, z(1-z), Q^2 = 0)$, in (2.5)[11].

(ii) Use the sum rule (2.1) and its GVD interpretation that associates the factor explicitly shown in (2.16) with the propagator of the $(q\bar{q})^{J=1}$ state of mass $M_{q\bar{q}} \equiv M$ and four-momentum squared $q^2 = -Q^2$. Simply put $Q^2 = 0$ in this propagator factor in (2.1), and evaluate the integral over M^2.

(iii) Use the symmetry between the incoming and the outgoing photon in the sum rule (2.1) for $\sigma_{\gamma_T^*}(W^2, Q^2)$, and accordingly put $Q^2 = 0$ in the diffractive forward-scattering amplitude appearing in (2.1) via the square root of the forward-scattering cross section (2.3).

Employing method (iii)[12], we note that the diffractive cross section (2.35) in the $Q^2 = 0$ limit reduces to[13]

$$\frac{d\sigma_{\gamma_T^*p \to (q\bar{q})_T^{J=1}p}}{dt dM^2} \bigg|_{t=0} (W^2, Q^2 = 0, M^2)$$

$$= \frac{1}{16\pi} \frac{\alpha R_{e^+e^-}}{3\pi} (\sigma^{(\infty)})^2 \begin{cases} \frac{1}{M^2}, & \text{for } M^2 < \Lambda^2(W^2), \\ 0, & \text{for } M^2 \geq \Lambda^2(W^2). \end{cases}$$

(3.1)

Rewriting (2.1) as a sum rule for the imaginary part of the forward-scattering amplitude for $\gamma^*p \to \gamma^*p$, we substitute (3.1), and upon squaring the result, we find

$$\frac{d\sigma_{\gamma^*p \to \gamma p}}{dt} \bigg|_{t=0} (W^2, Q^2)$$

$$= \frac{1}{16\pi} \left(\frac{\alpha R_{e^+e^-} \cdot \sigma^{(\infty)}}{3\pi} \right)^2 \left(\int_{m_0^2}^{\Lambda^2(W^2)} \frac{dM^2}{Q^2 + M^2} \right)^2 (1 + \beta_T^2),$$

(3.2)

or

---

[9] Note that $\Lambda^2(W^2)$ is related [21,2] to the gluon-structure function. As in case of the gluon-structure function, that depends on a more or less arbitrary input distribution, the free parameters in $\Lambda^2(W^2)$ cannot be theoretically derived at present.

[10] Helicity conservation is assumed.

[11] This approach approximates the imaginary part of the forward-scattering amplitude, i.e. the color-dipole cross section at $t_{\min} \neq 0$ by its value at $t = 0$, which value is identical to the one that enters the total virtual photoabsorption cross section. The approximation is well justified by the exceedingly small value of $|t_{\min}|$. Compare (3.16) below.

[12] For completeness, we also verified our result by using the technically somewhat more involved methods (i) and (ii)

[13] The (discontinuous) sudden vanishing of the cross section (3.1) for $M^2 \geq \Lambda^2(W^2)$ is an artefact of the δ-function ansatz (2.24).

$$\frac{d\sigma_{\gamma^*p\to\gamma p}}{dt}\bigg|_{t=0}(W^2, Q^2)$$

$$= \frac{1}{16\pi}\left(\frac{\alpha R_{e^+e^-}\sigma^{(\infty)}}{3\pi}\right)^2\left(\ln\frac{Q^2 + \Lambda^2(W^2)}{Q^2 + m_0^2}\right)^2(1 + \beta_T^2).$$
$$(3.3)$$

The factor $1 + \beta_T^2$ in (3.2) and (3.3) takes care of the real part of the forward-scattering amplitude. The correction β_T for the real part will not be discussed in detail, since it is expected to be fairly negligible, $\beta_T^2 \ll 1^{14}$, at least with respect to the accuracy of the presently available experimental data. A brief comment concerns the lower limit, m_0^2, in (3.2). As mentioned in connection with the results for the total cross section and for diffraction, a (correct) symmetric introduction of the threshold mass m_0 with respect to the incoming and outgoing photon leads to a correction term [19]. We have checked that this correction only insignificantly, at the 1% level, affects the very simple final result (3.3) for DVCS in the forward direction.

In the low-Q^2 limit of $Q^2 \ll \Lambda^2(W^2)$, we may represent (3.3) in terms of the scaling variable from (2.31),

$$\eta^{-1}(W^2, Q^2) = \frac{\Lambda^2(W^2)}{Q^2 + m_0^2}, \qquad (3.4)$$

to become

$$\frac{d\sigma_{\gamma^*p\to\gamma p}}{dt}\bigg|_{t=0}(W^2, Q^2)$$

$$= \frac{1}{16\pi}\left(\frac{\alpha R_{e^+e^-}\sigma^{(\infty)}}{3\pi}\right)^2 \cdot (\ln\eta^{-1})^2(1 + \beta_T^2), \quad (3.5)$$

or, upon introducing the total virtual photoabsorption cross section from (2.29) on the right-hand side in (3.5),

$$\frac{d\sigma_{\gamma^*p\to\gamma p}}{dt}\bigg|_{t=0}(W^2, Q^2) = \frac{1}{16\pi}\sigma_{\gamma^*p}^2(\eta)(1 + \beta_T^2) \quad (\eta \ll 1),$$
$$(3.6)$$

Even though $Q^2 = 0$ for the outgoing photon in DVCS, for $\Lambda^2(W^2) \gg Q^2$, according to (3.6), we nevertheless have approximate validity of the optical theorem; the imaginary part of the forward-scattering amplitude for $\gamma^*p \to \gamma p$ is in good approximation given by the imaginary part of the amplitude for $\gamma^*p \to \gamma^*p$. In the limit of real Compton scattering (3.6) becomes identical to the optical theorem for (real) Compton scattering,

$$\frac{d\sigma_{\gamma p\to\gamma p}}{dt}\bigg|_{t=0}(W^2) = \frac{1}{16\pi}\sigma_{\gamma p}^2(W^2)(1 + \beta_T^2). \qquad (3.7)$$

The transition from real Compton scattering to DVCS for $\eta \ll 1$, according to (3.7) and (3.6), corresponds to the substitution

$$\ln\frac{\Lambda^2(W^2)}{m_0^2} \to \ln\frac{\Lambda^2(W^2)}{Q^2 + m_0^2}. \qquad (3.8)$$

Turning to the opposite limit of $Q^2 \gg \Lambda^2(W^2)$, by expanding the logarithmic function in (3.3), we find

$$\frac{d\sigma_{\gamma^*p\to\gamma p}}{dt}\bigg|_{t=0}(W^2, Q^2)$$

$$= \frac{1}{16\pi}\left(\frac{\alpha R_{e^+e^-}\sigma^{(\infty)}}{3\pi}\right)^2\frac{\Lambda^4(W^2)}{Q^4}(1 + \beta_T^2)$$

$$= \frac{1}{16\pi}\left(\frac{\alpha R_{e^+e^-}\sigma^{(\infty)}}{3\pi}\right)^2\frac{1}{\eta^2}(1 + \beta_T^2). \qquad (3.9)$$

The approach to this limit (3.9) of a $1/Q^4$ dependence is slow, i.e. in the HERA energy range of $30\,\text{GeV} \lesssim W \lesssim 300\,\text{GeV}$, the behavior of (3.3) is closer to $1/Q^3$ (as found in the ZEUS experiment [5]) than to $1/Q^4$.

In (3.9), again we may introduce the virtual photoabsorption cross section, now inserting its asymptotic form from (2.30),

$$\frac{d\sigma_{\gamma^*p\to\gamma p}}{dt}\bigg|_{t=0}(W^2, Q^2)$$

$$= \frac{4}{16\pi}\sigma_{\gamma^*p}^2(W^2, Q^2)(1 + \beta_T^2)$$

$$= \frac{9}{16\pi}\sigma_{\gamma_T^*p}^2(W^2, Q^2)(1 + \beta_T^2) \quad (\text{for } Q^2 \gg \Lambda^2(W^2)).$$
$$(3.10)$$

According to (3.10), for asymptotic values of $Q^2 \gg \Lambda^2(W^2)$, the dependence on the kinematical variables of the forward-scattering amplitude for DVCS, $\gamma^*p \to \gamma p$, is determined by the amplitude for $\gamma^*p \to \gamma^*p$. The final photon being on-shell, $Q^2 = 0$, in (3.10) only leads to a constant, even though significant, enhancement factor with respect to what is obtained by applying the optical theorem to the amplitude for $\gamma^*p \to \gamma^*p$.

We may combine the limits (3.6) and (3.9) to conclude

$$\rho_T \equiv \frac{16\pi \frac{d\sigma_{\gamma^*p\to\gamma p}}{dt}\big|_{t=0}(W^2, Q^2)}{\sigma_{\gamma_T^*p}^2(W^2, Q^2)}$$

$$= \begin{cases} 1, & \text{for } Q^2 \ll \Lambda^2(W^2), \\ 9, & \text{for } Q^2 \gg \Lambda^2(W^2). \end{cases} \qquad (3.11)$$

If the transverse photoabsorption cross section in (3.11) is replaced by the total one, $\sigma_{\gamma^*}(W^2, Q^2)$, the factor 9 is replaced by 4. In Fig. 3, we show a plot of the ratio (3.11). The plot explicitly displays the enhancement due to putting the final photon on-shell in the square of the amplitude for $\gamma^*p \to \gamma^*p^{15}$. In Fig. 4, we have indicated the energy, $W = 89\,\text{GeV}$, at which the ratio in (3.11) was evaluated, even though the ratio is (obviously) independent of W in the limits indicated in (3.11).

---

[14] A recent estimate [25] in a color-dipole approach finds a value that decreases from about $\beta_T^2 \lesssim 0.2$ for $W \cong 30\,\text{GeV}$ to $\beta_T^2 \lesssim 0.1$ at $W \cong 300\,\text{GeV}$.

[15] The result (3.11) and Fig. 4 are based on the total cross section (2.27) to (2.30) that scales in η. Scaling in η is violated at large η for finite W, since the diffractive mass spectrum has an upper bound, m_1^2 [2]. Taking this effect into account leads to an enhancement of the ratio (3.11) in Fig. 4. The enhancement in Fig. 4 starts at $Q^2 \approx 50\,\text{GeV}^2$ and reaches about 10% at $Q^2 \approx 100\,\text{GeV}^2$.
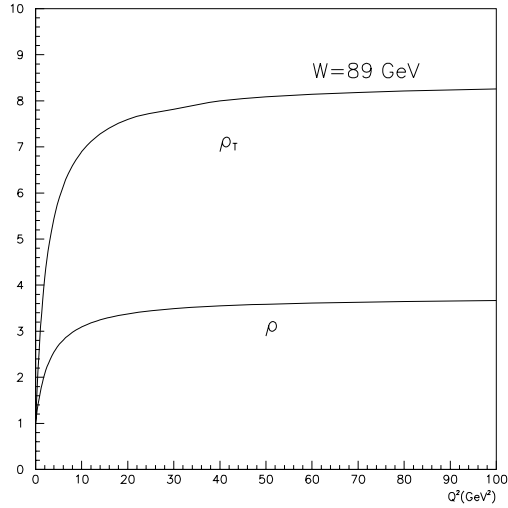
Fig. 3. The ratio $\rho_{\rm T}$ is calculated using the transverse part of the total photoabsorption cross section, $\rho_{\rm T} \equiv 16\pi {\rm d}\sigma(\gamma^*p \to \gamma p)/{\rm d}t \big/ \sigma^2_{\gamma^*_{\rm T}p}(W^2,Q^2)$, while ρ uses $\sigma_{\gamma^*p} \equiv \sigma_{\gamma^*_{\rm T}p} + \sigma_{\gamma^*_{\rm L}p}$, i.e. $\rho \equiv 16\pi {\rm d}\sigma(\gamma^*p \to \gamma p)/{\rm d}t \big/ \sigma^2_{\gamma^*p}(W^2,Q^2)$

The logarithmic behavior (3.5) that sets in for $\eta \ll 1$, leads to the conclusion that

$$\lim_{\substack{W \to \infty \\ Q^2 = {\rm const}}} \frac{\frac{{\rm d}\sigma_{\gamma^*p \to \gamma p}}{{\rm d}t}\Big|_{t=0}(W^2,Q^2)}{\frac{{\rm d}\sigma_{\gamma p \to \gamma p}}{{\rm d}t}\Big|_{t=0}(W^2)} = 1. \qquad (3.12)$$

The cross section for DVCS at any fixed Q^2 for sufficiently high energy, W, approaches the one of real Compton scattering. The result (3.12) is the Compton-scattering analogue of the asymptotic relationship (2.38) for the total photoabsorption cross section.

We emphasize that "saturation" in the sense of (2.38) and (3.12) does not depend on a specific "saturation-model" assumption. Saturation in the sense of (2.38) and
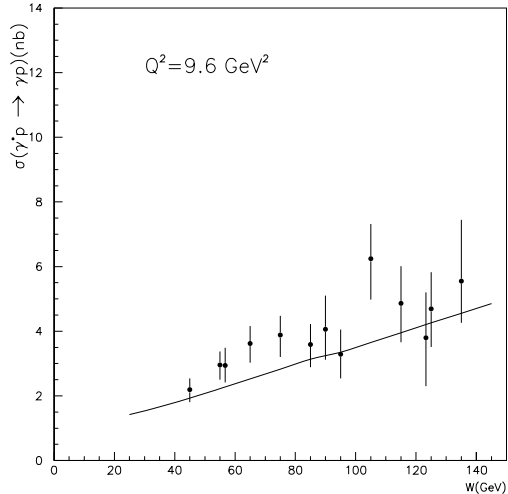
(3.12) only rests on the underlying two-gluon-exchange generic structure[16] from Fig. 1 that implies the basic relations (2.21) to (2.23).

The experiments [5] on $\gamma^*p \to \gamma p$ do not extract so far the forward-production cross section, nor the slope in momentum transfer. Theoretical considerations on the slope are beyond the scope of the present work. Assuming an exponential fall-off with slope b, $\exp(bt)$, we obtain from (3.3)

$$\sigma_{\gamma^*p \to \gamma p}(W^2,Q^2)$$
$$= \frac{1}{16\pi b}\left(\frac{\alpha R_{e^+e^-}\sigma^{(\infty)}}{3\pi}\right)^2 \left(\ln\frac{Q^2 + \Lambda^2(W^2)}{Q^2 + m_0^2}\right)^2 (1 + \beta_{\rm T}^2). \qquad (3.13)$$

In the comparison with the experimental data from HERA, we proceed in two steps. In the first step, we put

$$\beta_{\rm T} = 0, \quad b = 4 \ {\rm GeV}^{-2}. \qquad (3.14)$$

All other quantities in (3.13), the product $R_{e^+e^-}\sigma^{(\infty)}$, as well as $\Lambda^2(W^2)$ and m_0^2, were fixed by the analysis of the total cross section, $\sigma_{\gamma^*p}(W^2,Q^2)$. Compare (2.32) to (2.34).

When looking at the comparison with the experimental data in Figs. 4 and 5, the drastic assumption of a constant slope b in (3.14) has to be kept in mind, and the data indeed indicate[17] that the Q^2 dependence requires a decrease in b with increasing Q^2, as expected from the effective decrease of the dipole size $r_\perp$ with increasing Q^2 contained in the photon lightcone wave function (for the initial photon) in (2.5).
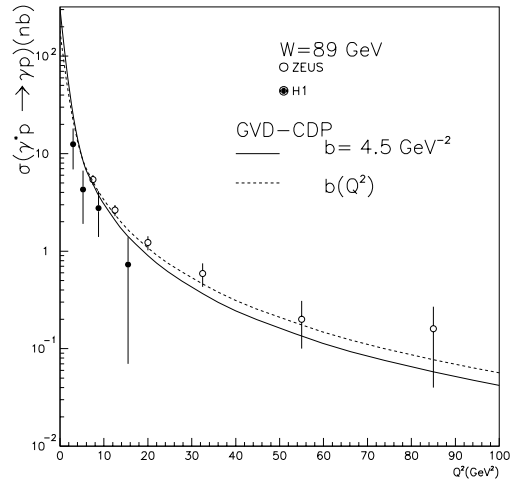

Fig. 5. As Fig. 4, but for the Q^2 dependence at fixed $W = 89\,{\rm GeV}$. The H1 data have been appropriately shifted [5] in energy from the H1 value of $W = 75\,{\rm GeV}$ to $W = 89\,{\rm GeV}$

---

[16] If anything in addition, it is the convergence of the integrals (2.22) and (2.23) over the distribution in the gluon momentum and its first moment that enters (2.38) and (3.12).

[17] This was previously observed by the ZEUS collaboration and in the theoretical analysis in [26].

Fig. 4. The W-dependence for DVCS for $Q^2 = 9.6\,{\rm GeV}^2$ compared with the prediction from the QCD-based GVD-CDP

In order to quantitatively estimate the influence of a change in slope with Q^2, we assume a dependence of $b(Q^2)$ on Q^2 extracted from ρ^0 electroproduction, even though the mass spectrum of the intermediate state coupled to the outgoing real photon extends quite far beyond the ρ^0 mass[18]. The fit to ρ^0 electroproduction gave [28] (in units of GeV^{-2})

$$b_{\rho_0}(Q^2) = \frac{3.46}{M_{\rho^0}^2 \left(1 + \frac{\left(Q^2/M_{\rho^0}^2\right)^{0.74}}{2.16}\right)} + 4.21. \qquad (3.15)$$

Numerically, according to (3.15), the slope b decreases from around $10\,GeV^{-2}$ at $Q^2 = 0$ to about $4.5\,GeV^{-2}$ at $Q^2 \cong 100\,GeV^2$. The effect of this change in slope is shown by the dotted line in Fig. 5.

In conjunction with the difference in slope between (3.14) and (3.15), the absolute normalization of the cross section was adjusted by including a real part of $\beta_T^2 = 0.1$ and by an increase of $\sigma^{(\infty)}$ by about 16%.

Altogether, the validity of the simple formula (3.3), without any adjusted parameter, is satisfactory and supports the underlying generic two-gluon-exchange structure from QCD. As mentioned, the ansatz (2.24) is a technical one that can be adopted without loss of generality. The specific form of $\Lambda^2(W^2)$ in (2.32) and (2.33) in the appropriate kinematic domain of $\eta \gg 1$ corresponds [2] to a simple assumption on the gluon distribution. An analogous assumption is inherently contained in any approach to DIS, usually in terms of an arbitrary input for the gluon distribution.

We end this section with a few comments on other approaches to DVCS.

Various approaches to DVCS, [29,30] and [31] start from the color-dipole formulation (2.11) for the total cross section that does not constrain the restriction in the color-dipole cross section to $(q\bar{q})^{J=1}p \rightarrow (q\bar{q})^{J=1}p$ transitions. The observed differences [13] between dipole cross sections leading to equivalent predictions for $\gamma^*p \rightarrow \gamma^*p$ and $\gamma^*p \rightarrow \gamma p$ are presumably due to $J \neq 1$ contributions. Both approaches of [29] and [30] use the energy, W, as the basic variable the dipole-cross section depends on, while [31] employs a dependence on the two variables x and Q^2.

References [29,30] both use a two-component approach (soft and hard pomeron) in the ansatz for the dipole cross section to accomodate both the $Q^2 \rightarrow 0$ and the $Q^2 \rightarrow \infty$ limits in distinction from our one-component approach (2.25) that describes the hard and the soft limit by the transition from $1/\eta$ to $\ln(1/\eta)$ according to (2.29) and (2.30). Our formulation is unique with respect to the simplicity of the final result for DVCS in (3.3) including the $Q^2 \ll \Lambda^2(W^2)$ and $Q^2 \gg \Lambda^2(W^2)$ limits in (3.5) and (3.9), and with respect to the transparent connection with the total photoabsorption cross section in (3.6) and (3.10).

The approach of the present paper and related work on DVCS based on the color-dipole picture [29] neglects

the effect of a non-zero minimal momentum transfer to the proton, $t_{\min}$, resulting from the difference in four-momentum squared of the incoming ($Q^2 > 0$) and outgoing photon ($Q^2 = 0$) in (forward) DVCS. For $\gamma^*p \rightarrow Xp$, in leading order in $(Q^2 + M_X^2)/W^2$,

$$t_{\min} \simeq -\frac{(Q^2 + M_X^2)^2}{W^4}M_p^2, \qquad (3.16)$$

where M_p denotes the proton mass. For DVCS, where $M_X^2 = 0$, we have $|t_{\min}| = x^2 M_p^2$, and, accordingly, $|t_{\min}|$ is of negligible magnitude with respect to all other dimensionful variables, since it lies between $10^{-2}\,GeV^2$ at $x = 10^{-1}$ and $10^{-8}\,GeV^2$ at $x = 10^{-4}$. The effect of $P' \neq P$, where P and P' refer to the incoming and outgoing nucleon, respectively, has been investigated by generalizing parton distributions and evolution equations to this case of $P' \neq P$ [32,33]. Generalized parton distributions (GPD's) can thus be predicted at any Q^2, once they have been specified at an input scale, Q_0^2, by an appropriate parameterization. For DVCS see [34,27,26]. A comparison of the theoretical prediction thus obtained [26,5] for the Q^2 dependence of DVCS with ours in Fig. 5 reveals no drastic difference. A theoretical analysis of (forward) DVCS that only relies on those parameters that are fixed by measurements of $\sigma_{\gamma^*p}(W^2, Q^2)$, thus ignoring the change in four-momentum of the proton, $P \neq P'$, so far seems adequate for a representation of the available experimental data on DVCS.

4 Vector-meson electroproduction

Using the results for diffractive production, $\gamma^*p \rightarrow (q\bar{q})^{J=1}p$, of the $(q\bar{q})^{J=1}$ continuum collected in (2.35) to (2.37) in Sect. 2, and applying quark–hadron duality, it is now a simple matter to arrive at a parameter-free prediction for vector-meson forward production.

Quark–hadron duality [7] says that the asymptotic cross section for e^+e^- annihilation into a quark–antiquark pair, $e^+e^- \rightarrow q\bar{q}$, interpolates the production of the low-lying vector mesons of the corresponding quark flavor. That is, the integrals over the low-lying vector-meson peaks in e^+e^- annihilation, when averaged over an interval ΔM_V^2 determined by the vector-meson level spacing, become identical to the low-energy continuation of the asymptotic cross sections for $e^+e^- \rightarrow q\bar{q}$ with appropriate flavor of the quark q.

For the case of diffractive production, quark–hadron duality allows us to determine the cross section for vector-meson production by integration of the cross sections (2.35) to (2.37) for the diffractively produced $(q\bar{q})^{J=1}$ continuum[19],

---

[18] An estimate of the ρ^0 contribution to DVCS gave a contribution of the order of 20% [27] at low Q^2, rapidly decreasing with increasing Q^2.

[19] Compare also [9] for the application of quark–hadron duality to vector-meson production. Also, we note that a refined treatment should simultaneously analyze quark–hadron duality in e^+e^- annihilation and diffractive production.

$$\frac{d\sigma_{\gamma^*p\to(q\bar{q})_{M(V)}^{J=1}p}}{dt}\bigg|_{t=0}(W^2,Q^2)$$
$$=\int dz\int_{\Delta M_V^2}dM^2\frac{d\sigma_{\gamma^*p\to(q\bar{q})^{J=1}p}}{dtdM^2dz}\bigg|_{t=0}(W^2,Q^2,M^2).$$
$$(4.1)$$

In (4.1), $\gamma^*p\to(q\bar{q})_{M(V)}^{J=1}p$, may refer to the sum of transverse and longitudinal cross sections, as well as to transverse and longitudinal cross sections separately, whereby γ^* has to be replaced by γ_T^* and γ_L^*, respectively[20]. The mass of the vector meson V is denoted by $M(V)\equiv M_V$, and the quark flavor of the cross section on the right-hand side in (4.1) has to be identical to the quark content of the vector meson, i.e. when substituting (2.35) to (2.37) into (4.1), $R_{e^+e^-}$ is to be replaced by

$$R_{e^+e^-}=3\sum_q Q_q^2\to\begin{cases}R^{(\rho^0)}=\frac{9}{10}R^{(\rho^0+\omega)}=\frac{3}{2},\\R^{(\omega)}=\frac{1}{10}R^{(\rho^0+\omega)}=\frac{1}{6},\\R^{(\phi)}=R^{(\Upsilon)}=\frac{1}{3},\\R^{(J/\psi)}=\frac{4}{3}.\end{cases}\quad(4.2)$$

When predicting vector-meson production according to (4.1), we have to discriminate between the low-lying vector mesons, ρ,ω,ϕ, that may be described by the limit of vanishing quark mass, $m_u=m_d=m_s=0$, and the vector mesons, J/ψ and Υ, where the approximations $M_{J/\psi}^2\approx 4m_c^2$ and $M_\Upsilon^2\approx 4m_b^2$ are appropriate. In Sect. 4.1 we treat the light vector mesons by inserting (2.35) to (2.37) into (4.1). For the treatment of the heavy vector mesons in Sect. 4.2, we shall generalize (2.35) to (2.37) to the case of massive quarks. A comparison with the experimental data will be given in Sect. 4.3.

4.1 Massless quarks, ρ^0, ω, ϕ production

Before giving the explicit result obtained by integration of (4.1), it will be illuminating to consider the approximation of (4.1)

$$\frac{d\sigma_{\gamma^*p\to(q\bar{q})_{M(V)}^{J=1}p}}{dt}\bigg|_{t=0}(W^2,Q^2)$$
$$\simeq\Delta M_V^2\int dz\frac{d\sigma_{\gamma^*p\to(q\bar{q})^{J=1}p}}{dtdM^2dz}\bigg|_{t=0}(W^2,Q^2,M^2=M_V^2),$$
$$(4.3)$$

and determine its behavior for $Q^2\to\infty$ and $Q^2\to 0$ upon inserting the cross sections from (2.35) to (2.37) at $M^2=M_V^2$.

The cross sections (2.35) to (2.37), with respect to Q^2, dominantly depend on the variable Q^2+M^2. We first of all consider the limit of

$$Q^2+M_V^2\gg\Lambda^2(W^2).\quad(4.4)$$

___

[20] We restrict ourselves to evaluating $\gamma_T^*p\to(q\bar{q})_T^{J=1}p$ and $\gamma_L^*p\to(q\bar{q})_L^{J=1}p$, i.e. by disregarding transitions such as $\gamma_T^*p\to(q\bar{q})_L^{J=1}p$, we assume helicity conservation.

For definiteness, we note that according to (2.32)

$$2\,\mathrm{GeV}^2\lesssim\Lambda^2(W^2)\lesssim 7\,\mathrm{GeV}^2\quad(4.5)$$

for the energy range covered by HERA of $30\,\mathrm{GeV}\lesssim W\lesssim 300\,\mathrm{GeV}$. From the leading term in the expansion of (2.37) in powers of $\Lambda^2(W^2)/(Q^2+M_V^2)$, upon insertion in (4.3) we find

$$\frac{d\sigma_{\gamma^*p\to(q\bar{q})_{M(V)}^{J=1}p}}{dt}\bigg|_{t=0}(W^2,Q^2,M_V^2)$$
$$=\frac{1}{16\pi}\frac{\alpha R^{(V)}}{3\pi}(\sigma^{(\infty)}(W^2))^2\frac{\Lambda^4(W^2)\Delta M_V^2}{(Q^2+M_V^2)^3}\frac{Q^2}{Q^2+M_V^2}.\ (4.6)$$

The transverse-production cross section, from the expansion of (2.35), is given by

$$\frac{d\sigma_{\gamma_T^*p\to(q\bar{q})_{M(V)T}^{J=1}p}}{dt}\bigg|_{t=0}(W^2,Q^2,M_V^2)$$
$$=\frac{1}{16\pi}\frac{\alpha R^{(V)}}{3\pi}(\sigma^{(\infty)}(W^2))^2$$
$$\cdot\frac{4\Lambda^4(W^2)M_V^2\Delta M_V^2}{(Q^2+M_V^2)^4}\left(\frac{Q^2}{Q^2+M_V^2}\right)^2.\quad(4.7)$$

The results (4.6) and (4.7), according to (4.4), are not only valid for the production of light vector mesons, but their range of validity also includes the case of the continuum of heavy $q\bar{q}$ states formed from light quarks with

$$M_V^2\equiv M_{q\bar{q}}^2\gg\Lambda^2(W^2),\quad(4.8)$$

where (4.4) is valid even for $Q^2\geq 0$.

We turn to $\rho^0(\omega,\phi)$ production, where (4.4) with (4.5) requires

$$Q^2\gg\Lambda^2(W^2)\quad(4.9)$$

since $\Lambda^2(W^2)>M_{\rho^0(\omega,\phi)}^2$. The unpolarized cross section (4.6) in this case may be more appropriately written as

$$\frac{d\sigma_{\gamma^*p\to(q\bar{q})_{M(V)}^{J=1}p}}{dt}\bigg|_{t=0}(W^2,Q^2,M_V^2)$$
$$=\frac{1}{16\pi}\frac{\alpha R^{(V)}}{3\pi}(\sigma^{(\infty)}(W^2))^2\frac{\Lambda^4(W^2)\Delta M_V^2}{(Q^2+M_V^2)^3}$$
$$\left(V=(\rho^0,\omega,\phi);\ Q^2\gg\Lambda^2(W^2)>M_{\rho^0,\omega,\phi}^2\right).\ (4.10)$$

Since the transverse cross section (4.7) is suppressed by a power of $Q^2+M_V^2$, the longitudinal cross section in its leading term coincides with (4.6) and the longitudinal-to-transverse ratio in the asymptotic limit (4.4) is given by

$$R_{\mathrm{L/T}}=\frac{Q^2}{4M_V^2}\qquad(Q^2\gg\Lambda^2(W^2)>M_V^2).\quad(4.11)$$

For the opposite limit of

$$Q^2+M_V^2\ll\Lambda^2(W^2),\quad(4.12)$$

by expansion of (2.37), and integration from M_1^2 to $M_1^2 + \Delta M_V^2$, we find

$$
\left.\frac{\mathrm{d}\sigma_{\gamma^*p\to(q\bar q)^{J=1}p}}{\mathrm{d}t}\right|_{t=0}(W^2,Q^2,M_V^2)
$$

$$
= \frac{1}{16\pi}\frac{\alpha R^{(V)}}{3\pi}(\sigma^{(\infty)}(W^2))^2 \ln\left(1+\frac{\Delta M_V^2}{Q^2+M_1^2}\right). \quad (4.13)
$$

A final remark concerns the energy dependence of the whole diffractively produced $(q\bar q)^{J=1}$ continuum in the limit (4.12), relevant for photoproduction of light quarks, $q = u,d,s$ at HERA energies. With (3.1), we find,

$$
\int_{m_0^2} \mathrm{d}M^2 \left.\frac{\mathrm{d}\sigma_{\gamma^*p\to(q\bar q)_{\mathrm T}^{J=1}p}}{\mathrm{d}t\mathrm{d}M^2}\right|_{t=0}(W^2,Q^2=0,M^2)
$$

$$
= \frac{1}{16\pi}\frac{\alpha R_{e^+e^-}}{3\pi}\left(\sigma^{(\infty)}(W^2)\right)^2 \int_{m_0^2}^{\Lambda^2(W^2)}\frac{\mathrm{d}M^2}{M^2}
$$

$$
= \frac{1}{16\pi}\frac{\alpha R_{e^+e^-}}{3\pi}\left(\sigma^{(\infty)}(W^2)\right)^2 \ln\frac{\Lambda^2(W^2)}{m_0^2}. \quad (4.14)
$$

While the energy dependence in photoproduction of a discrete vector-meson state (4.13) is even weaker than the energy dependence of the total photoproduction cross section, the energy dependence of the whole $(q\bar q)^{J=1}$ continuum, with the approximate constancy of $\sigma^{(\infty)}(W^2)$, shows the logarithmic dependence of $\sigma_{\gamma p}(W^2)$ from (2.29).

We finally give the expressions for the vector-meson-production cross section obtained by evaluating the quark–hadron-duality relation (4.1) without further approximation. Upon insertion of (2.35) to (2.37), and integration over $\mathrm{d}z$ and $\mathrm{d}M^2$, we find

$$
\left.\frac{\mathrm{d}\sigma_{\gamma^*p\to(q\bar q)^{J=1}_{M(V)}p}}{\mathrm{d}t}\right|_{t=0}(W^2,Q^2)
$$

$$
= \frac{1}{16\pi}\frac{\alpha R^{(V)}}{3\pi}\left(\sigma^{(\infty)}\right)^2\left[\Pi(\Lambda^2(W^2),Q^2,M^2)\right]_{M_1^2}^{M_2^2}, \quad (4.15)
$$

where the function $\Pi(\Lambda^2(W^2),Q^2,M^2)$ is to be evaluated at the limits of M_1^2 and M_2^2, where

$$
\Delta M_V^2 = M_2^2 - M_1^2,
$$
$$
M_1^2 < M_V^2 < M_2^2. \quad (4.16)
$$

For the case of the sum of transverse- and longitudinal-production cross sections, we have

$$
\Pi(\Lambda^2(W^2),Q^2,M^2)
$$
$$
= +\frac{1}{2}\ln\frac{(\Lambda^2+Q^2)(\sqrt X+Q^2+\Lambda^2)+M^2(Q^2-\Lambda^2)}{\sqrt X+M^2+Q^2-\Lambda^2}
$$
$$
-\frac{\Lambda^2}{\sqrt{\Lambda^2(4Q^2+\Lambda^2)}}
$$
$$
\cdot\ln\frac{\sqrt{\Lambda^2(4Q^2+\Lambda^2)}\sqrt X+\Lambda^2(3Q^2-M^2+\Lambda^2)}{M^2+Q^2}, \quad (4.17)
$$

while for the longitudinal and the transverse case, separately,

$$
\Pi_{\mathrm L}(\Lambda^2(W^2),Q^2,M^2)
$$
$$
= -\frac{1}{M^2+Q^2}+\frac{1}{2\sqrt{Q^2\Lambda^2}}\arctan\frac{M^2+Q^2-\Lambda^2}{2\sqrt{Q^2\Lambda^2}}
$$
$$
+\frac{2}{\sqrt{\Lambda^2(4Q^2+\Lambda^2)}}
$$
$$
\cdot\ln\frac{\sqrt{\Lambda^2(4Q^2+\Lambda^2)}\sqrt X+\Lambda^2(3Q^2-M^2+\Lambda^2)}{M^2+Q^2}, \quad (4.18)
$$

where Λ^2 stands for $\Lambda^2(W^2)$ and X is given by

$$
X \equiv (Q^2+M^2-\Lambda^2)^2+4Q^2\Lambda^2, \quad (4.19)
$$

and

$$
\Pi_{\mathrm T}(\Lambda^2(W^2),Q^2,M^2)
$$
$$
= \frac{Q^2}{M^2+Q^2}-\frac{1}{2}\sqrt{\frac{Q^2}{\Lambda^2}}\arctan\frac{M^2+Q^2-\Lambda^2}{2\sqrt{Q^2\Lambda^2}}
$$
$$
+\frac{1}{2}\ln\frac{(\Lambda^2+Q^2)(\sqrt X+Q^2+\Lambda^2)+M^2(Q^2-\Lambda^2)}{\sqrt X+M^2+Q^2-\Lambda^2}
$$
$$
-\frac{2Q^2+\Lambda^2}{\sqrt{\Lambda^2(4Q^2+\Lambda^2)}}
$$
$$
\cdot\ln\frac{\sqrt{\Lambda^2(4Q^2+\Lambda^2)}\sqrt X+\Lambda^2(3Q^2-M^2+\Lambda^2)}{M^2+Q^2}. \quad (4.20)
$$

Upon adopting an exponential t-dependence, $\exp(b_V t)$, the cross section for vector-meson production, $\sigma_{\gamma^*p\to(q\bar q)^{J=1}_{M(V)}p}(W^2,Q^2)$, is obtained from (4.3) and (4.15) by multiplication by $1/b_V$.

For the case of the ρ^0 meson we have compared the results of the integration of (4.1) given by (4.15) with the approximate results for large Q^2 in (4.10) and for small Q^2 in (4.13). With $M_{\rho^0}^2 = 0.59\,\mathrm{GeV}^2$ and $\Delta M_{\rho^2}^2 = 1\,\mathrm{GeV}^2$ and the lower bound $M_1^2 = 0.36\,\mathrm{GeV}^2$ in (4.15), we find that the large-Q^2 approximation for $Q^2 \geq 90\,\mathrm{GeV}^2$ in (4.10) overestimates the exact evaluation of (4.1) by less than 10%. With decreasing Q^2 the large-Q^2 approximation substantially overestimates the exact evaluation, since (4.4) becomes violated and in addition the approximation of $Q^2 + M^2$ by a constant, $Q^2 + M_V^2$, becomes less justified. For $Q^2 \to 0$, the approximation (4.13) exceeds the exact evaluation by a few percent. Altogether, for semi-quantitative discussions, the approximations (4.10) and (4.13) are very useful, while for detailed comparison with the experimental data the results based on (4.15) should be employed.

4.2 Massive quarks, J/ψ and Υ production

The light-cone wave functions (2.8) and (2.9) include a non-zero rest mass, m_q, of the quark. There are essentially two important effects, when passing from the approximation of massless quarks, relevant for ρ^0, w, ϕ production, where $M_V^2 \gg 4m_q^2 \cong 0$, to massive quarks, relevant for J/ψ and Υ production, where $M_V^2 \cong 4m_q^2 \neq 0$.

First of all, the transition from massless to massive quarks affects the lightcone variable z. In the massless-quark case, we have

$$0 \leq z \leq 1, \tag{4.21}$$

and z is related to the angle of the $q\bar{q}$ axis relative to the photon-direction in the $q\bar{q}$ rest frame via

$$\sin\theta = 2\sqrt{z(1-z)},$$
$$\cos\theta = 1 - 2z. \tag{4.22}$$

In the case of massive quarks, (2.18), the range of z for given quark mass and given mass $M_{q\bar{q}}$ is determined by

$$M^2 \equiv M_{q\bar{q}}^2 = \frac{m_q^2}{z(1-z)}. \tag{4.23}$$

One finds

$$z_- \leq z \leq z_+,$$
$$z_\pm = \frac{1}{2} \pm \frac{1}{2}\sqrt{1 - 4\frac{m_q^2}{M_{q\bar{q}}^2}}, \tag{4.24}$$

and an integration over dz is restricted to the interval

$$\Delta z = z_+ - z_- = \sqrt{1 - 4\frac{m_q^2}{M_{q\bar{q}}^2}} = \begin{cases} 1, & \text{for } m_q^2 = 0, \\ 0, & \text{for } m_q^2 = \frac{1}{4}M_{q\bar{q}}^2. \end{cases} \tag{4.25}$$

Upon introducing the variable y defined by

$$z = (z_+ - z_-)y + z_- = \begin{cases} z_+, & \text{for } y = 1, \\ z_-, & \text{for } y = 0, \end{cases} \tag{4.26}$$

the integration over dz in the massive-quark case is represented by

$$\int_{z_-}^{z_+} dz = \sqrt{1 - \frac{4m_q^2}{M_{q\bar{q}}^2}} \int_0^1 dy. \tag{4.27}$$

For later reference, we note the integral over the threshold factor in (4.27),

$$\Delta F^2(m_q^2, \Delta M_V^2)$$
$$\equiv \int_{4m_q^2}^{4m_q^2+\Delta M_V^2} dM^2 \sqrt{1 - \frac{4m_q^2}{M^2}} \int_0^1 dy$$
$$= (4m_q^2 + \Delta M_V^2)\sqrt{\frac{\Delta M_V^2}{4m_q^2 + \Delta M_V^2}}$$
$$+ 2m_q^2 \ln \frac{1 - \sqrt{\frac{\Delta M_V^2}{4m_q^2+\Delta M_V^2}}}{1 + \sqrt{\frac{\Delta M_V^2}{4m_q^2+\Delta M_V^2}}}. \tag{4.28}$$

In passing, we mention that the $q\bar{q}$ rest-frame angle in the massive case is related to y by

$$\sin\theta = 2\sqrt{y(1-y)},$$
$$\cos\theta = 1 - 2y. \tag{4.29}$$

Moreover, in terms of y,

$$z(1-z) = \frac{m_q^2}{M^2} + \left(1 - \frac{4m_q^2}{M^2}\right)y(1-y),$$
$$z^2 + (1-z)^2 = \frac{2m_q^2}{M^2} + \left(1 - \frac{4m_q^2}{M^2}\right)(y^2 + (1-y)^2), \tag{4.30}$$

such that y is indeed the appropriate generalization of the variable z to the massive-quark case.

The second important modification with respect to the massless-quark case concerns the diffractive production cross sections (2.35) to (2.37) when passing from $M_V^2 \gg 4m_q^2 \cong 0$ to $M_V^2 \cong 4m_q^2 \neq 0$. For $q\bar{q}$ production near threshold this modification may be accomplished by a simple substitution to be applied in the sum of the transverse and the longitudinal cross section for the massless-quark case given in (2.35) and (2.36).

To derive the substitution prescription, we consider the sum of the transverse and the longitudinal lightcone wave function given in (2.8) and (2.9), respectively, and compare the massive case, $m_q^2 \neq 0$, with the massless one, $m_q^2 = 0$. We find that at production threshold, where

$$M_{q\bar{q}}^2 = 4m_q^2, \quad z(1-z) = \frac{1}{4}, \tag{4.31}$$

the sum of the transverse and longitudinal wave functions of the massive case is recovered from the massless one by carrying out the substitution

$$Q^2 \to Q^2 + 4m_q^2, \tag{4.32}$$

in the expression for the massless case. For a vector meson at or closely above threshold, the quark mass according to (4.32) acts as an additive contribution to Q^2 of magnitude $4m_q^2 \cong M_V^2$. When applying the substitution (4.32) to the sum of the diffractive-production differential cross sections for the massless-quark case in (2.35) and (2.36) at $z(1-z) = \frac{1}{4}$, the mass $M^2 \equiv \mathbf{k}_\perp^2/z(1-z)$ in (2.35) and (2.36) must be put to zero, in order to correctly realize the threshold relation (4.31). Finally upon substitution, the threshold mass, $4m_q^2$, is to be replaced by the vector-meson mass, i.e.

$$(4m_c^2, 4m_b^2) \to (M_{J/\psi}^2, M_\Upsilon^2). \tag{4.33}$$

In order to obtain an approximate expression for the production cross section in the case of $M_V^2 \cong 4m_q^2$ when applying quark–hadron duality according to (4.1), we will use (4.27) and (4.28), while approximating the $(q\bar{q})^{J=1}$ production cross sections (2.35) and (2.36) upon substitution of (4.32) by their values at threshold, $4m_q^2$, whereby we identify threshold and vector-meson mass, $4m_q^2 = M_V^2$.

Upon having carried out the preceeding steps in the sum of the cross sections (2.35) and (2.36), and upon substituting (4.28), we find that (4.1) is approximated by

$$
\begin{aligned}
\left.\frac{d\sigma_{\gamma^* p \to V p}}{dt}\right|_{t=0} &= \left.\frac{d\sigma_{\gamma_T^* p \to V_T p}}{dt}\right|_{t=0} + \left.\frac{d\sigma_{\gamma_L^* p \to V_L p}}{dt}\right|_{t=0} \\
&= \frac{3}{2} \cdot \frac{\alpha R^{(V)}}{3 \cdot 16\pi^2} (\sigma^{(\infty)})^2 \\
&\quad \cdot \int_{4m_q^2}^{4m_q^2 + \Delta M_V^2} dM^2 \sqrt{1 - \frac{4m_q^2}{M^2}} \, (Q^2 + M_V^2) \\
&\quad \cdot \left(\frac{1}{Q^2 + M_V^2} - \frac{1}{Q^2 + M_V^2 + \Lambda^2(W^2)}\right)^2, \quad (4.34)
\end{aligned}
$$

where $V = J/\psi, \Upsilon$. The integration over dM^2 in (4.34) runs from the threshold, $4m_q^2$, to the upper limit $4m_q^2 + \Delta M_V^2$, where ΔM_V^2 is determined by the vector-meson level spacing and $4m_q^2 \le M_V^2 \le 4m_q^2 + M_V^2$.

The integrand in (4.34) is easily verified to be identical to what one obtains by applying the substitution (4.32) only to the longitudinal-production cross section (2.36). In fact, one finds that the transverse cross section (2.35) vanishes upon applying the substitution procedure based on (4.32).

Identifying the longitudinal cross section in (4.34) via its Q^2 dependence, (4.34) may be rewritten as

$$
\begin{aligned}
&\left.\frac{d\sigma_{\gamma_T^* p \to V_T p}}{dt}\right|_{t=0} + \left.\frac{d\sigma_{\gamma_L^* p \to V_L p}}{dt}\right|_{t=0} \\
&= \left.\frac{d\sigma_{\gamma_L^* p \to V_L p}}{dt}\right|_{t=0} \left(1 + \frac{M_V^2}{Q^2}\right), \quad (4.35)
\end{aligned}
$$

i.e. the longitudinal-to-transverse ratio fulfills

$$
R_{L/T} = \frac{Q^2}{M_V^2} \quad (\text{for } Q^2 \ge 0). \quad (4.36)
$$

This ratio differs from the one in the massless-quark case (4.11) by the missing factor $1/4$ and by the range of validity in Q^2.

The final expression for the production cross section (4.34) becomes

$$
\begin{aligned}
&\left.\frac{d\sigma_{\gamma^* p \to V p}}{dt}\right|_{t=0} \\
&= \frac{3}{2} \cdot \frac{\alpha R^{(V)}}{3 \cdot 16\pi^2} (\sigma^{(\infty)})^2 \frac{\Lambda^4(W^2)}{(Q^2 + M_V^2)^3} \frac{1}{\left(1 + \frac{\Lambda^2(W^2)}{Q^2 + M_V^2}\right)^2} \\
&\quad \cdot \Delta F^2(m_q^2, \Delta M_V^2) \quad (V = J/\psi, \Upsilon), \quad (4.37)
\end{aligned}
$$

where $\Delta F^2(m_q^2, \Delta M_V^2)$ is given by (4.28). Note that this expression for the cross section is independent of an assumption on the relative magnitude of $Q^2 + M_V^2$ and $\Lambda^2(W^2)$, in distinction from the massless-quark case, where (4.13) as well as (4.6) and (4.10) are relevant, respectively, for $Q^2 + M_V^2 \ll \Lambda^2(W^2)$ and $Q^2 + M_V^2 \gg \Lambda^2(W^2)$. The additional factor $3/2$ in the massive-quark

case relative to the massless one is a genuine consequence of the fact that $4m_q^2 \cong M_V^2$ for the heavy vector mesons. While according to (4.31), for massive quarks $z(1-z) = 1/4$, for massless quarks the integration over $z(1-z)$ yield $1/6$. In addition to the factor $3/2$ and the factor R^V, for $Q^2 + M_V^2 \gg \Lambda^2(W^2)$, the massless and the massive case differ by the replacement of ΔM_V^2 by $\Delta F^2(m_q^2, \Delta M_V^2)$.

We point out a few outstanding features of the (approximate) result (4.37) and its massless-quark counterparts (4.10) and (4.13). Rather than referring to the massless-quark and the massive-quark case, we will refer to the ρ^0 case and the J/ψ case, where ρ^0 stands for ρ^0, ω, ϕ and J/ψ stands for J/ψ and Υ. From (4.37), as well as (4.10) and (4.13), we conclude to the following.

(i) The cross sections for ρ^0 as well as J/ψ production are functions of $Q^2 + M_V^2$, rather than Q^2 itself. When plotted against $Q^2 + M_V^2$, one will find approximately the same functional behavior for the ρ^0 and the J/ψ, except for normalization differences due to $R^{(V)}$ (compare (4.2)), the above-mentioned factor $3/2$, and the effective value of ΔM_V^2. In the ρ^0 case, ΔM_V^2 corresponds to the level spacing, while for the J/ψ the analogous quantity is determined by the integral over the threshold factor (4.28).

(ii) As soon as

$$
Q^2 + M_V^2 \gg \Lambda^2(W^2) \quad (4.38)
$$

the energy dependence is "hard", as $\Lambda^4(W^2)$. This condition for the J/ψ is fulfilled already for Q^2 not far from $Q^2 \ge 0$ at HERA energies, while $Q^2 \gg \Lambda^2(W^2)$ is required for the ρ^0. Note that far beyond HERA energies, the increase of $\Lambda^2(W^2)$ with energy will result in a soft energy dependence at $Q^2 \cong 0$ for the J/ψ since (4.38) will be violated, and the J/ψ according to (4.37) will behave as the ρ^0 in photoproduction at presently available energies. To stress the point again: it is relation (4.38) that decides on the energy dependence. A ρ^0-like continuum state of sufficiently high mass (consisting of approximately massless u and d quarks) according to (4.6) shows a "hard" energy behavior even in the limit of $Q^2 < \Lambda^2(W^2)$. On the other hand, a hypothetical quark of mass $m_q \cong 1\,\text{GeV}$ forming a bound state of about $2\,\text{GeV}$ would violate (4.38) for $Q^2 \to 0$ and sufficiently high energy, and accordingly the energy dependence would be soft.

So far we have considered the approximate evaluation of the quark–hadron-duality relation (4.1). For the direct evaluation of (4.1) in the massive-quark case, we need the generalization of (4.35) to (4.37) to massive quarks even beyond the threshold (4.31). Employing the light-cone wave functions (2.8) and (2.9) for a non-vanishing quark mass we have gone through the steps that lead to (2.35) to (2.37) in the massless case. Upon substituting the result into (4.1), and upon integration over dM^2 from $m_q^2/z(1-z)$ to $4m_q^2 + \Delta M_V^2$, one obtains

Table 1. We show the input parameters used in the calculations of ρ^0, J/ψ and Υ production, as well as the enhancement of J/ψ and Υ production relative to ρ^0 production in the approximate evaluation and in the exact numerical evaluation of quark–hadron duality. The enhancements of J/Ψ and Υ refer to identical values of $Q^2 + M_V^2 = 89.48\,\text{GeV}^2$

V	$R^{(\rho^0)}/R^{(V)}$	M_V (GeV)	ΔM_V^2(GeV^2)	m_q (GeV)	$E^{(V)}_{\text{appr.}}$	$E^{(V)}$
ρ^0	1	0.77	1.0	0	—	—
J/ψ	$\frac{9}{8}$	3.096	4.0	1.5	2.01	2.25
Υ	$\frac{9}{2}$	9.460	11.0	4.6	3.32	2.69

$$
\left.\frac{\mathrm{d}\sigma_{\gamma^*p\to(J/\psi,\Upsilon)p}}{\mathrm{d}t}\right|_{t=0}
$$

$$
= \frac{\alpha R^{(J/\psi,\Upsilon)}}{32\pi^2}(\sigma^{(\infty)})^2 \int_{\frac{1}{2}(1-\overline{\Delta z})}^{\frac{1}{2}(1+\overline{\Delta z})}\mathrm{d}z
$$

$$
\cdot \Bigg[\left(z^2 + (1-z)^2\right)
$$

$$
\cdot \Pi_{\mathrm{T}}\left(\Lambda^2(W^2), Q^2 + \frac{m_q^2}{z(1-z)}, M^2 - \frac{m_q^2}{z(1-z)}\right)
$$

$$
+ \left(4Q^2 z(1-z) + \frac{m_q^2}{z(1-z)}\right)
$$

$$
\cdot \Pi_{\mathrm{L}}\left(\Lambda^2(W^2), Q^2 + \frac{m_q^2}{z(1-z)},\right.
$$

$$
\left.\left.M^2 - \frac{m_q^2}{z(1-z)}\right)\right]_{\frac{m_{(c,b)}^2}{z(1-z)}}^{4m_{(c,b)}^2 + \Delta M_{(J/\psi,\Upsilon)}^2} \tag{4.39}
$$

Here the functions Π_{T} and Π_{L} are identical to the ones encountered earlier in the massless cases, (4.20) and (4.18), respectively. The arguments in (4.34), however, differ from the ones in (4.20) and (4.18) by the substitution[21]

$$
Q^2 \to Q^2 + \frac{m_q^2}{z(1-z)},
$$

$$
M^2 \to M^2 - \frac{m_q^2}{z(1-z)}. \tag{4.40}
$$

The interval $\overline{\Delta z}$ in (4.39) is related to the one that is given in (4.25) by the replacement of $M_{q\bar{q}}^2$ by $4m_q^2 + \Delta M_V^2$, i.e.

$$
\overline{\Delta z} = \sqrt{\frac{\Delta M_{(J/\psi,\Upsilon)}^2}{4m_{(c,b)}^2 + \Delta M_{(J/\psi,\Upsilon)}^2}} \tag{4.41}
$$

For the sake of clarity, we mention that (4.39) is to be understood under the constraint

$$
4m_{(c,b)}^2 \le M_{(J/\psi,\Upsilon)}^2 \le 4m_{(c,b)}^2 + \Delta M_{(J/\psi,\Upsilon)}^2, \tag{4.42}
$$

[21] Note that the substitution (4.40) at the threshold (4.31) coincides with the substitution (4.32). At threshold, the massive-quark *cross section* is obtained from the massless one by applying the substitution (4.40). This is not true in general, as the factor in front of $\prod_{\mathrm{L}}$ in general is *not* obtained by the substitution (4.40).

where $M_{(J/\psi,\Upsilon)}$ denotes the experimental value of the vector-meson mass, and $\Delta M_{(J/\psi,\Upsilon)}^2$ the level spacing, while the mass of charm or bottom quark, $m_{(c,b)}$, is not uniquely fixed.

We have compared the numerical result from (4.39) with the approximate one in (4.37). For J/ψ production, for $Q^2 + M_{J/\psi}^2 \ge 25\,\text{GeV}^2$, the approximation (4.37) overestimates the result from (4.39) by less than 10%. For the case of Υ production, for $Q^2 \cong 0$, for later reference we note that the approximation result is about 40% larger than the result of the exact evaluation.

In order to compare the cross sections for J/ψ and Υ production with the cross sections for ρ^0 production, it is useful to remove the effect due to differences in the quark content and to define an "enhancement factor" $E^{(V)}$ by

$$
E^{(V)} \equiv \frac{R^{(\rho^0)}}{R^{(V)}}\frac{\sigma_{\gamma^*p\to Vp}}{\sigma_{\gamma^*p\to\rho^0 p}}, \qquad V = J/\psi, \Upsilon, \tag{4.43}
$$

where the cross sections are to be evaluated at identical fixed values of $Q^2 + M_V^2$ for the different vector mesons and at the same energy W. For $Q^2 + M_V^2$ sufficiently large, the slope parameters of the t-distribution, $b(Q^2 + M_V^2)$, are experimentally known to become identical, $b(Q^2 + M_V^2 \gtrsim 30\,\text{GeV}^2) \cong 4.5\,\text{GeV}^{-2}$, and (4.43) may be evaluated by inserting forward-production cross sections. Inserting the approximations (4.37) and (4.10), we have

$$
E^{(V)}_{\text{appr.}} = \frac{3}{2}\frac{\Delta F^2(m_q^2, \Delta M_V^2)}{\Delta M_{\rho^0}^2}\cdot\frac{1}{\left(1 + \frac{\Lambda^2(W^2)}{Q^2 + M_V^2}\right)^2},
$$

$$
V = J/\psi, \Upsilon. \tag{4.44}
$$

The dependence on $Q^2 + M_V^2$ leads to some increase of $E^{(J/\psi)}$ with $Q^2 + M_V^2$ that is confirmed by the more reliable evaluation of (4.43) based on (4.39) and (4.15). The enhancement (4.43) and (4.44) is recognized as a genuine massive-quark effect with respect to the factor $3/2$ following from $4m_q^2 \cong M_V^2$, and the threshold factor $\Delta F^2(m_q^2, \Delta M_V^2)$ that replaces ΔM_V^2 in the massive-quark case.

We have numerically evaluated (4.43), assuming a universal slope parameter b for ρ^0, J/ψ and Υ. Inserting (4.39) and (4.15), we find the enhancement factor of Table 1 at $W = 90\,\text{GeV}$ and $Q^2 + M_V^2 = 89.48\,\text{GeV}^2$ that is relevant for Υ photoproduction. In Table 1, we also present the

results obtained from the approximation (4.44). The deviation from the results from (4.43) for the J/ψ is due to the mentioned excess of about 10% of the approximation (4.10) for the ρ^0 meson with respect to the exact result. The larger deviation in the case of the Υ is largely due to the above mentioned 40% deviation of (4.37) for the Υ.

4.3 Comparison with experiment

In this section we compare the Q^2 dependence, the W dependence and the absolute normalization of the vector-meson-production cross sections with the experimental data.

From (4.10) and (4.37) the Q^2 dependence of vector-meson production at $Q^2 + M_V^2 \gg \Lambda^2(W^2)$ is determined by $(Q^2 + M_V^2)^{-n}$ where $n = 3$. A fit to the experimental data [35] for ρ^0 production including data from $Q^2 \cong 10\,\mathrm{GeV}^2$ to $Q^2 \cong 50\,\mathrm{GeV}^2$ leads to $n_{\rho^0} = 2.60 \pm 0.04$. For J/ψ production, a fit in the interval $12\,\mathrm{GeV}^2 \leq Q^2 + M_{J/\psi}^2 \leq 60\,\mathrm{GeV}^2$ by the ZEUS collaboration gave $n_{J/\psi} = 2.72 \pm 0.10$ [36]. Both n_{ρ^0} and $n_{J/\psi}$ are consistent with the prediction of $n = 3$, taking into account the fairly low value of the lower end of the interval in $Q^2 + M_V^2$ used in the fits. It only exceeds $\Lambda^2(W \cong 70\,\mathrm{GeV}) \cong 3.5\,\mathrm{GeV}^2$ by a factor of 3.

Both the H1 and the ZEUS collaborations have fitted the energy dependence of their data by a simple power law,

$$\sigma_{\gamma^* p \to V p}(W^2, Q^2) \sim W^{\delta^{(V)}(Q^2)}. \qquad (4.45)$$

We have compared our theoretical energy dependence to the power law (4.45) by adapting our energy dependence to this power-law form in a restricted energy range (chosen as in the experiments) via

$$\delta^{(V)}(Q^2 + M_V^2) = \frac{1}{\ln \frac{W_2}{W_1}} \ln \frac{\sigma_{\gamma^* p \to V p}(W_2, Q^2 + M_V^2)}{\sigma_{\gamma^* p \to V p}(W_1, Q^2 + M_V^2)}. \qquad (4.46)$$

The consistency of our prediction with the experimental data [6,37] for ρ^0 and J/ψ production is shown in Fig. 6.

We turn to the absolute normalization of the vector-meson-production cross section. According to (4.10) and (4.13) as well as (4.37) the normalization is first of all determined by the product of $R^{(V)} \cdot (\sigma^{(\infty)})^2$, where $R^{(V)}$ according to (4.2) contains the charges of the relevant quark flavors, and $\sigma^{(\infty)}$ denotes the asymptotic value of the (universal) color-dipole cross section (2.21). In Table 1, according to (4.2), we show the frequently used ratio $R^{(\rho^0)}/R^{(V)}$ that normalizes the cross sections to the ρ^0 case as far as the quark content of the vector mesons is concerned. For the universal dipole cross section, $\sigma^{(\infty)}$, we use

$$\sigma^{(\infty)} = 68\,\mathrm{GeV}^{-2} = 27.5\,\mathrm{mb}. \qquad (4.47)$$

This value is consistent with the value from the analysis of $\sigma_{\gamma^* p}(W^2, Q^2)$, compare (2.34). In addition to $R^{(V)}$ and $\sigma^{(\infty)}$, the normalization of the cross sections in (4.10), (4.13) and (4.37) is determined by the integration interval
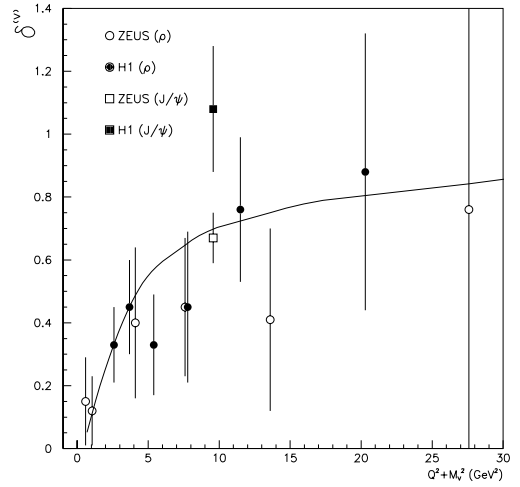

Fig. 6. The exponent $\delta^{(V)}$ in a parameterization of the energy dependence of the experimental cross section by $W^{\delta^{(V)}(Q^2 + M_V^2)}$ compared with the predictions from the QCD-based GVD-CDP

ΔM_V^2 entering via quark–hadron duality as well as the mass of the respective quark. The interval ΔM_V^2 follows from the vector-meson level spacing, and for the ρ^0, in the approximate treatment (4.10) and (4.13), $\Delta M_{\rho^0}^2 = 1\,\mathrm{GeV}^2$ directly multiplies the diffractive-production cross section at $M^2 \equiv M_{\rho^0}^2$. In the massive quark case, the integrated threshold factor $\Delta F^2(m_q^2, \Delta M_V^2)$ from (4.28), effectively replaces ΔM_V^2. In Table 1, we have collected all relevant quantities, including the quark masses.

Finally, the experimental cross sections include an integration over the (exponential) t dependence, $\exp(bt)$, that implies a factor of $1/b$. We note that [35,28]

$$b_{\rho^0}(Q^2 + M_\rho^2 \cong M_{J/\psi}^2) \cong 5.5\,\mathrm{GeV}^{-2},$$
$$b_{J/\psi}(Q^2 + M_{J/\psi}^2 \cong M_{J/\psi}^2) \cong 4.5\,\mathrm{GeV}^{-2}, \qquad (4.48)$$

while for lower values of $Q^2 + M_V^2$, b_{ρ^0} increases to

$$b_{\rho^0}(Q^2 + M_{\rho^0}^2 \cong 1\,\mathrm{GeV}^2) \cong 7.5\,\mathrm{GeV}^{-2}. \qquad (4.49)$$

With these preparations, it is a simple matter to discuss the relative normalization of ρ^0, J/ψ and Υ production. For the ratio of J/Ψ photoproduction ($Q^2 = 0$) to ρ^0 production at $Q^2 + M_{\rho^0}^2 = M_{J/\Psi}^2$, from (4.15), (4.39) and (4.48), we find

$$\frac{9}{8}\sigma^{(J/\psi)}/\sigma^{(\rho^0)} = 1.42, \qquad (4.50)$$

while for Υ photoproduction, from Table 1

$$E^{(\Upsilon)} = \frac{9}{2}\sigma^{(\Upsilon)}/\sigma^{(\rho^0)} = 2.69. \qquad (4.51)$$

The factors (4.50) and (4.51) are consistent with the enhancements found experimentally for J/ψ [38] as well as Υ production [39]. Note that a replacement of the integrated
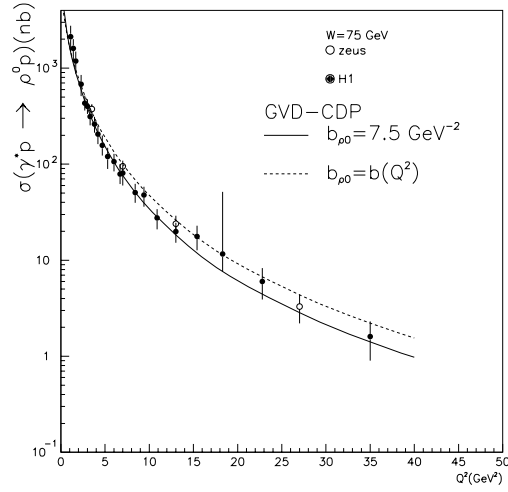
Fig. 7. The Q^2 dependence of ρ^0 production, $\gamma^* p \to \rho^0 p$, at fixed $W = 75\,\mathrm{GeV}$, compared with the predictions from the QCD-based GVD-CDP for $b_{\rho 0} = 7.5\,\mathrm{GeV}^{-2}$ and a Q^2-dependent slope, $b_{\rho^0}(Q^2)$ from (3.15)

threshold factor (4.28) by the level spacings would have led to drastically increased enhancements.

In Figs. 7 to 10, we show a comparison of our predictions with the experimental Q^2 and W dependence of ρ^0 and J/ψ production. The theoretical results shown in the figures are based on the use of (4.1) without further approximation, i.e. they are based on (4.15) for the ρ^0 and on (4.39) for the J/ψ. For ρ^0 production, for Fig. 7 we inserted a constant slope parameter

$$b_{\rho^0} = 7.5\,\mathrm{GeV}^{-2}, \qquad (4.52)$$

as well as the Q^2-dependent slope [28] from (3.15). In Fig. 8, we show the W dependence of ρ^0 production at various values of Q^2 compared with data from ZEUS and H1 measurements [6]. In Fig. 9, we show the longitudinal-to-transverse ratio for ρ^0 production. According to Figs. 7 to 9, we have satisfactory agreement for the Q^2 and W dependence, including normalization, as well as the longitudinal-to-transverse ratio. In Fig. 10 we show the

comparison with photoproduction of J/ψ mesons. The agreement in the W dependence is very satisfactory indeed.

We conclude that our two-gluon-exchange QCD-based color-dipole approach (called GVD-CDP) yields a parameter-free representation (except for using the experimental value of the slope parameter b) of vector-meson production. The dependence on the variable $Q^2 + M_V^2$ is a strict consequence of including the quark mass of magnitude $4m_q^2 \cong M_V^2$ into the lightcone wave function of the photon. The effective value of the gluon transverse momentum, $\Lambda^2(W^2)$, sets the scale for the large, $Q^2 + M_V^2 \gg \Lambda^2(W^2)$, and small, $Q^2 + M_V^2 \ll \Lambda^2(W^2)$, regimes with associated strong and weak W dependences. The relative normalizations of the cross sections are a genuine consequence of the quark masses relative to the vector-meson masses; for the ρ^0 the approximation of massless quarks is relevant, while for the J/ψ and Υ we have $M_{J/\psi}^2 \cong 4m_c^2$ and $M_\Upsilon^2 \cong 4m_b^2$, respectively.

4.4 A brief reference to the literature on vector-meson photo- and electroproduction

The first theoretical papers on electroproduction of vector mesons [16,40] some thirty-four years ago were based on (simple diagonal) vector-meson dominance with s-channel helicity conservation. From the coupling of the vector meson to a conserved source as required by electromagnetic current conservation, it was concluded that production by longitudinal photons should dominate the cross section via $R_{\mathrm{L/T}} \sim Q^2/M_V^2$ – a prediction that has stood the test of time and also appears in our present paper. The unpolarized cross section, however, was predicted [16,40] to only decrease as $1/Q^2$ in strong disagreement with present-day experimental results that require an asymptotic behavior approximately as $1/Q^6$. A revival [41] of off-diagonal GVD [42] implied a $1/Q^4$ dependence for the unpolarized cross section that in fact was found [41] to be consistent with the experimental data up to around $Q^2 \le 20\,\mathrm{GeV}^2$ available at the time, including the ratio of $R_{\mathrm{L/T}}$. Since the traditional vector dominance approach relies on (soft) pomeron
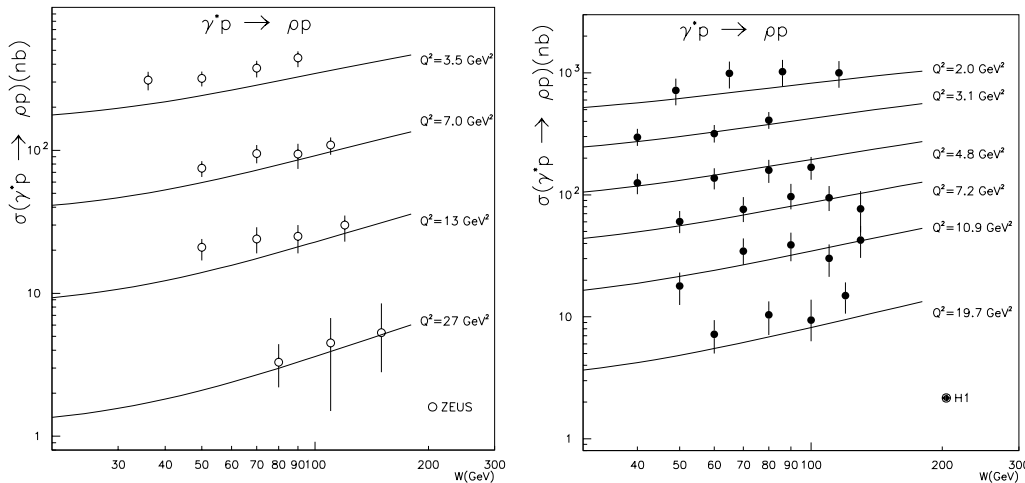

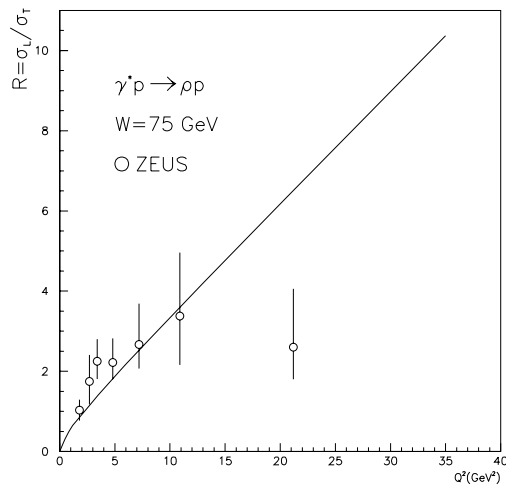**Fig. 8.** The W dependence of ρ^0 production for various values of Q^2 compared with the QCD-based GVD-CDP

Fig. 9. The longitudinal-to-transverse ratio, $R_{L/T}$ for $\gamma^* p \to \rho^0 p$ as a function of Q^2

exchange, it is unable to describe the strong W dependence observed for sufficiently large values of $Q^2 + M_V^2$.

The modern QCD theory of vector-meson production uses the notion of the pomeron as a two-gluon-exchange object [3] throughout. Various approaches differ in their application of methods from pQCD [43, 44], pQCD combined with quark–hadron duality [9], the use of non-perturbative QCD approaches [45–47] and combinations of both [27,48]. The pQCD approach, valid at sufficiently high Q^2 led to an asymptotic $(1/Q^6)\alpha_s(Q^2)xg(x,Q^2)$ behavior of the dominant longitudinal cross section [44], closely related to our asymptotic behavior as $(1/Q^6)\sigma^{(\infty)}\Lambda^2(W^2)$. In its spirit more closely related to our approach are the investigations in [9] in so far as they make use of quark–hadron duality, however in conjunction with conventional parameterizations of the gluon structure function.
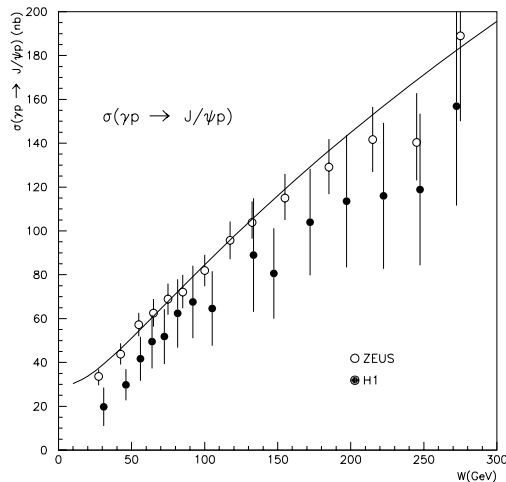

Fig. 10. The W dependence of the J/ψ photoproduction cross section, compared with the theoretical prediction from the QCD-based GVD-CDP

A very detailed account of diffractive vector-meson production based on suitably extrapolating the unintegrated gluon density into the low-Q^2 domain is given in [23]. The treatment [23] goes beyond our treatment in so far as it provides a refined description of the dependence of the vector-meson wave function for light and heavy vector mesons rather than relying on quark–hadron duality. The agreement with experiment of the present work indicates that the Q^2 and W dependence is fairly insensitive to details of the vector-meson wave function.

The approach of the present paper is applicable at all $Q^2 \geq 0$ for light and heavy vector mesons. The increase of the saturation scale with energy, $\Lambda^2(W^2)$, determined from the DIS measurements of the total photoabsorption and expressed in terms of three fit parameters is sufficient to yield a parameter-free and unambiguous description of (forward) vector-meson production. The final expressions for the cross sections are simple and transparent, and they put the (approximate) universal dependence on $Q^2 + M_V^2$, as well as the W dependence and the relative normalization of the cross sections for the production of different vector mesons on a firm footing.

5 Conclusion

After many years of experimental and theoretical efforts, it seems that a coherent picture of DIS in the low x diffraction region, DVCS, and vector-meson production has emerged. The Q^2 dependence and the relative normalization of the cross sections is well understood from our QCD-based approach of the GVD-CDP. Also the scale for the remarkable transition from a soft to a hard energy dependence in DIS, DVCS and vector-meson production, the saturation scale $\Lambda^2(W^2)$, as well as the very occurrence of this transition, is understood, even though an ab initio prediction of the power of W responsible for the increase with energy, W, is beyond the scope of the present investigation.

References

1. M. Kuroda, D. Schildknecht, Phys. Rev. D **66**, 094005 (2002)
2. M. Kuroda, D. Schildknecht, Phys. Rev. D **67**, 094008 (2003)
3. F.E. Low, Phys. Rev. D **12**, 163 (1975); S. Nussinov, Phys. Rev. Lett. **34**, 1286 (1975); Phys. Rev. D **14**, 246 (1976); J. Gunion, D. Soper, Phys. Rev. D **15**, 2617 (1977)
4. N.N. Nikolaev, B.G. Zhakharov, Z. Phys. C **49**, 607 (1991); Z. Phys. C **53**, 331 (1992); Sov. Phys. JETP **78**, 598 (1994)
5. H1 Collaboration, C. Adloff et al., Phys. Lett. B **517**, 47 (2001); ZEUS Collaboration, S. Chekanov et al., DESY 03-059
6. H1 Collaboration, C. Adloff et al., Eur. Phys. J. C **13**, 371 (2000); C **10**, 373 (1999); ZEUS Collaboration, J. Breitweg et al., Eur. Phys. J. C **6**, 603 (1999)

7. J.J. Sakurai, Phys. Lett. B **46**, 207 (1973); Proceedings 1973 International School of Subnuclear Physics, Erice, Italy, edited by A. Zichichi Academic Press, N.Y.), p. 219; D. Schildknecht, F. Steiner, Phys. Lett. B **56**, 36 (1975)

8. B. Gorczyca, D. Schildknecht, Phys. Lett. B **47**, 71 (1973); R. Devenish, D. Schildknecht, Phys. Rev. D **19**, 93 (1976)

9. E.M. Levin, A.D. Martin, M.G. Ryskin, T. Teubner, Z. Phys. C **74**, 671 (1997); A.D. Martin, M.G. Ryskin, T. Teubner, Phys. Rev. D **55**, 4329 (1997); D **62**, 014022 (2000)

10. J.D. Bjorken, J. Kogut, D.E. Soper, Phys. Rev. D **3**, 1382 (1971)

11. V.S. Fadin, E.A. Kuraev, L.N. Lipatov, Phys. Lett. B **60**, 50 (1975); Ya. Balitskii, L.N. Lipatov, Sov. J. Nucl. Phys. **28**, 822 (1978)

12. I.P. Ivanov, N.N. Nikolaev, Phys. Rev. D **65**, 054004 (2002)

13. S. Donnachie, G. Dosch, P. Landshoff, O. Nachtmann, Pomeron physics and QCD (Cambridge University Press 2002), p. 282

14. J.J. Sakurai, D. Schildknecht, Phys. Lett. B **40**, 121 (1972)

15. D. Schildknecht, H. Spiesberger, Acta Phys. Pol. B **29**, 1261 (1998)

16. H. Fraas, D. Schildknecht, Nucl. Phys. B **14**, 543 (1969)

17. G. Cvetic, D. Schildkencht, A. Shoshi, Eur. Phys. J. C **13**, 301 (2000)

18. L. Frankfurt, V. Guzey, M. Strikman, Phys. Rev. D **58**, 094039 (1998)

19. G. Cvetic, D. Schildknecht, B. Surrow, M. Tentyukov, Eur. Phys. J. C **20**, 77 (2001)

20. ZEUS 96/97: ZEUS Collaboration, S. Chekanov et al., Eur. Phys. J. C **21**, 443 (2001); ZEUS Collaboration, M. Derrick et al., Z. Phys. C **72**, 399 (1996);
ZEUS SVTX 95: ZEUS Collaboration, J. Breitweg et al., Eur. Phys. J. C **7**, 609 (1999); ZEUS BPC 95: ZEUS Collaboration, J. Breitweg et al., Phys. Lett. B **407**, 432 (1997); ZEUS BPT 97: ZEUS Collaboration, J. Breitweg et al., Phys. Lett. B **487**, 53 (2000); H1 SVTX 95: H1 Collaboration, C. Adloff et al., Nucl. Phys. B **497**, 3 (1997); H1 96/97: H1 Collaboration, C. Adloff et al., Eur. Phys. J. C **21**, 33 (2001); H1 97: H1 Collaboration, C. Adloff et al., Eur. Phys. J. C **13**, 609 (2000)

21. D. Schildknecht, in Diffraction 2000, Nucl. Phys. (Proc. Suppl.) **99**, 121 (2001); D. Schildknecht, B. Surrow, M. Tentyukov, Phys. Lett. B **499**, 116 (2001)

22. D. Schildknecht, B. Surrow, M. Tentyukov, Mod. Phys. Lett. A **16**, 1829 (2001); D. Schildknecht, in The 9th International Workshop on Deep Inelastic Scattering, DIS 2001, Bologna, Italy, edited by G. Bruni et al. (World Scientific 2002) p. 798

23. I.P. Ivanov, hep-ph/0303053; JETP Lett. **69**, 294 (1999)

24. K. Prytz, Phys. Lett. B **311**, 286 (1993)

25. L. Favart, M.V.T. Machado, DESY 03-016, hep-ph/0302079

26. A. Freund, M. McDermott, M. Strikman, Phys. Rev. D **67**, 036001 (2003); A. Freund, M. McDermott, Phys. Rev. D **65**, 091901 (2002); A. Freund, hep-ph/0306012

27. A. Donnachie, J. Gravelis, G. Show, Eur. Phys. J. C **18**, 539 (2001)

28. A. Kreisel, Talk presented at LISHEP 2002, Workshop on diffractive physics, February 2002, Rio de Janeiro, hep-ex/0208013

29. H. Donnachie, H.G. Dosch, Phys. Lett. B **502**, 74 (2001)

30. J.R. Forshaw, G. Kerley, G. Shaw, Phys. Rev. D **60**, 074012 (1999)

31. M. McDermott, R. Sandapen, G. Shaw, Eur. Phys. J. C **22**, 655 (2002)

32. X. Ji, Phys. Rev. Lett. **78**, 610 (1997); Phys. Rev. D **55**, 7114 (1997); A.V. Radyushkin, Phys. Rev. D **56**, 5524 (1997); K.J. Golec-Biernat, A.D. Martin, Phys. Rev. D **59**, 014029 (1999)

33. J.C. Collins, A. Freund, Phys. Rev. D **59**, 074009 (1999)

34. L.L. Frankfurt, A. Freund, M. Strikman, Phys. Rev. D **58**, 114001 (1998); Erratum D **59**, 119901 (1999)

35. X. Janssen, Contribution to DIS 2000, Acta Phys. Pol. B **33**, 3529 (2002)

36. J. Tandler, Contribution to DIS 2003, St. Petersburg, April 2003

37. H1 Collaboration, C. Adloff et al., Phys. Lett. B **483**, 23 (2000); ZEUS Collaboration, S. Chekanov et al., Eur. Phys. J. C **24**, 345 (2002)

38. A. Levy, Contribution to DIS 2002, Acta Phys. Pol. B **33**, 3547 (2002)

39. ZEUS Collaboration, J. Breitweg et al., Phys. Lett. B **437**, 432 (1998); H1 Collaboration, C. Adloff et al., Phys. Lett. B **483**, 23 (2000)

40. C.F. Cho, G.J. Gounaris, Phys. Rev. **186**, 1619 (1969)

41. D. Schildknecht, A. Schuler, B. Surrow, Phys. Lett. B **449**, 328 (1999)

42. H. Fraas, B.J. Read, D. Schildknecht, Nucl. Phys. B **86**, 346 (1975), Nucl. Phys. B **88**, 301 (1975)

43. M.G. Ryskin, Z. Phys. C **57**, 89 (1993)

44. S.J. Brodsky, L. Frankfurt, J.F. Gunion, A.H. Mueller, M. Strikman, Phys. Rev. D **50**, 3134 (1994)

45. A. Donnachie, P.V. Landshoff, Phys. Lett. B **185**, 403 (1987); Erratum B **198**, 590 (1987); Nucl. Phys. B **311**, 509 (1989); Phys. Lett. B **437**, 408 (1998)

46. J.R. Cudell, I. Royon, Phys. Lett. B **397**, 317 (1997)

47. H.G. Dosch, E. Ferreira, Eur. Phys. J. C **29**, 45 (2003)

48. A. Donnachie, J. Gravelis, G. Shaw, Phys. Rev. D **63**, 114013 (2001)